AD-A038 502 ARMY ELECTRONICS COMMAND FORT MONMOUTH N J F/G 17/5
EFFECTS OF CLOUD PARTICLES ON REMOTE SENSING FROM SPACE IN THE --ETC(U)
JAN 77 R D LOW

UNCLASSIFIED ECOM-5811 NL

| OF |
AD
A038502

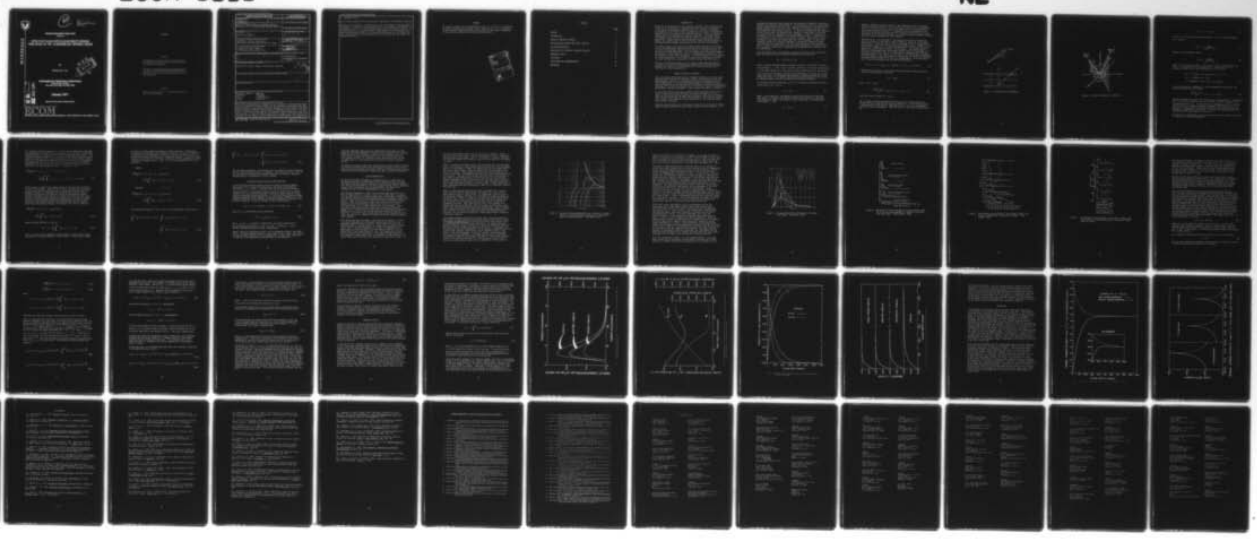

END

DATE
FILMED
5-77

RESEARCH AND DEVELOPMENT TECHNICAL REPORT
ECOM-5811

EFFECTS OF CLOUD PARTICLES ON REMOTE SENSING FROM SPACE IN THE 10-MICROMETER INFRARED REGION

By

Richard D.H. Low

Atmospheric Sciences Laboratory
US Army Electronics Command
White Sands Missile Range, New Mexico 88002

January 1977

Approved for public release; distribution unlimited.

ECOM
UNITED STATES ARMY ELECTRONICS COMMAND - FORT MONMOUTH, NEW JERSEY 07703

NOTICES

Disclaimers

The findings in this report are not to be construed as an official Department of the Army position, unless so designated by other authorized documents.

The citation of trade names and names of manufacturers in this report is not to be construed as official Government indorsement or approval of commercial products or services referenced herein.

Disposition

Destroy this report when it is no longer needed. Do not return it to the originator.

SECURITY CLASSIFICATION OF THIS PAGE *(When Data Entered)*

REPORT DOCUMENTATION PAGE

READ INSTRUCTIONS BEFORE COMPLETING FORM

1. REPORT NUMBER: ECOM-5811	2. GOVT ACCESSION NO.
3. RECIPIENT'S CATALOG NUMBER	
4. TITLE *(and Subtitle)*: EFFECTS OF CLOUD PARTICLES ON REMOTE SENSING FROM SPACE IN THE 10-MICROMETER INFRARED REGION.	5. TYPE OF REPORT & PERIOD COVERED
	6. PERFORMING ORG. REPORT NUMBER
7. AUTHOR(s): Richard D. H. Low	8. CONTRACT OR GRANT NUMBER(s)
9. PERFORMING ORGANIZATION NAME AND ADDRESS: Atmospheric Sciences Laboratory, White Sands Missile Range, New Mexico 88002	10. PROGRAM ELEMENT, PROJECT, TASK AREA & WORK UNIT NUMBERS: DA Task No. 1T1 61101A 91A
11. CONTROLLING OFFICE NAME AND ADDRESS: US Army Electronics Command, Fort Monmouth, New Jersey 07703	12. REPORT DATE: January 1977
	13. NUMBER OF PAGES: 51
14. MONITORING AGENCY NAME & ADDRESS *(if different from Controlling Office)*: Research and development technical rept.	15. SECURITY CLASS. *(of this report)*: UNCLASSIFIED
	15a. DECLASSIFICATION/DOWNGRADING SCHEDULE

16. DISTRIBUTION STATEMENT *(of this Report)*

Approved for public release; distribution unlimited.

17. DISTRIBUTION STATEMENT *(of the abstract entered in Block 20, if different from Report)*

18. SUPPLEMENTARY NOTES

19. KEY WORDS *(Continue on reverse side if necessary and identify by block number)*

Radiative transfer	Radiance
IR window	Blackbody
Cloud	Transmissivity
Aerosol	Emissivity

20. ABSTRACT *(Continue on reverse side if necessary and identify by block number)*

This report, the second of a proposed series of reports on the mesoscale application of satellite infrared imagery and its theoretical background, describes the derivation of the radiative transfer equation and its solution by the Gauss-Seidel iteration method in a more lucid and elementary manner than is usually found in the books in the hope that those whose interest lies only in the application aspect of satellite imagery may find this report helpful and useful. On the basis of microphysical and climatological considerations, four cloud models representing one stratus type and three cumulus types were investigated as to

next page

DD FORM 1 JAN 73 1473 EDITION OF 1 NOV 65 IS OBSOLETE

037 620

SECURITY CLASSIFICATION OF THIS PAGE *(When Data Entered)*

20. ABSTRACT (cont)

their optical properties and the thickness requirements for blackbody radiation.

Findings are as follows: (1) Reflection in the 10-micrometer infrared region is negligible; (2) Given the same microstructure, a cloud appears more "black" in the windows of the 11- to 13-micrometer region than in any other windows in this infrared region; (3) In satellite work, cloud emissivity (or transmissivity) should be calculated on the basis of upwelling radiances; and (4) Cloud liquid water content may be a better parameter in defining thickness requirement for blackbody radiation.

PREFACE

The author expresses his deep appreciation to Dr. K. N. Liou of the University of Utah for his meticulous review of this report and to Dr. R. L. Armstrong of the New Mexico State University for his advice on the complex mathematics of the scattering phase function and the Mie parameters.

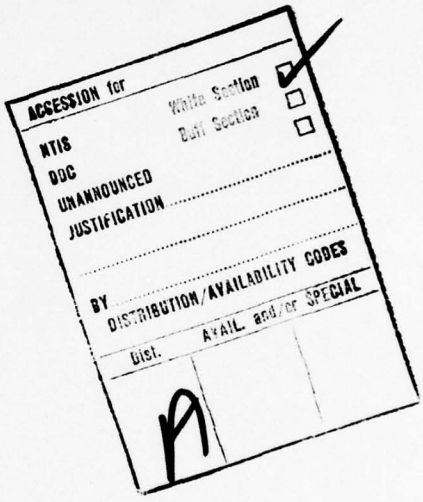

CONTENTS

INTRODUCTION

Underlying the measurement of the upwelling radiation from a ground or sea surface or a cloud layer by a meteorological satellite such as SMS/GOES 1 is the theory of atmospheric radiative transfer. Without a reasonable understanding of the ramifications attendant to this theory, interpretation and analysis of the radiance data from the satellite, either in streams or imagery, would be inadequate or completely erroneous. The importance of the SMS/GOES series to many Army missions such as air operations, target acquisition, terminal homing, and the detection and tracking of severe weather was already noted in the first report, "Mesoscale Determination of Cloud-Top Height: Problems and Solutions," and will not be reiterated.

The present report, the second of a proposed series of papers on the theoretical and experimental applications of satellite observations, will deal in a more understandable manner with the theory of radiative transfer as applied to a cloudy atmosphere. Next, the report will show how the equation of radiative transfer may be solved for a nonhomogeneous atmosphere, with brief mention of some other techniques. Since this equation is to be applied to cloudy atmospheres, a brief exposition of cloud microstructure is then in order with particular attention to stratiform and cumuliform clouds.

Finally, a detailed examination will be made of under what microphysical conditions a cloud may be unmistakeably regarded as a blackbody radiator and what this implies in the determination of cloud-top heights and in retrieval of surface temperatures.

THEORY OF RADIATIVE TRANSFER

There are several well-known books on radiative transfer [1,2,3] and a vast amount of open literature and technical reports too numerous to cite here. Chandrasekhar's book [1] is prepared primarily for the astrophysicists in their investigation of stellar atmospheres; Goody [2] provides excellent reference materials on the calculation of atmospheric transmission functions; Kondratyev [3] is more comprehensive and will be found useful in meteorological applications, though less rigorous in his treatment of radiative transfer.

In this short section, the author summarizes the experiences gained in his study of radiative transfer and hopes to present the theory in a lucid manner so that anyone who has been barely exposed to the problems of radiative transfer may be able to follow the exposition. There will be nothing new or fresh in this approach to the theory; many of the ideas are drawn from previous literature.

Radiative transfer theory is a quantitative study of the transfer of radiant energy through a medium which can scatter, absorb, and emit radiation. In

representing radiative energy, there are two often-used radiometric quantities: radiance and irradiance (or emittance). In astrophysics, they are, respectively, specific intensity and specific flux. Radiance or intensity is defined as the energy radiated from a source per unit time per unit projected area per unit solid angle per unit spectral interval. In satellite meteorology, when referred to the infrared band, the physical unit radiance is often given in milliwatt per square meter per steradian per unit wavenumber. Spectral irradiance (or emittance) or flux is defined as the energy irradiated upon or emitted from a unit surface per unit time per unit spectral interval. The physical unit of irradiance is milliwatt per square meter per unit wavenumber. In the solar radiation region, it is usually expressed in calorie per minute per square centimeter per unit wavelength. The total flux density of solar radiation, which is given in calorie per minute per square centimeter or langley per minute, as used in meteorology, is obtained by integrating solar irradiance over all wavelengths.

With these definitions, the equation of radiative transfer along an arbitrary path according to the law of energy conservation can be written

$$dI_\lambda = -\beta_e I_\lambda \, ds + j_\lambda \, ds \quad , \tag{1}$$

where I_λ denotes the monochromatic radiance, a function of position, direction, and wavelength λ; β_e the volume extinction coefficient, a function of wavelength; s is the path length; and j_λ the source function coefficient to be determined, also a function of position, direction, and wavelength. The first term on the right side of Eq. (1) represents the reduction of radiation energy due to the extinction process in the medium, whereas the second term denotes the increase of radiation energy carried by scattering and emission processes.

The volume extinction coefficient β_e (cm^{-1}) is related to the mass extinction coefficient k_e (g^{-1} cm^2) by

$$\beta_e = \rho \, k_e \quad , \tag{2}$$

where ρ is the density of the medium in which the extinction of radiation takes place. In general, the extinction coefficient consists of two radiation components; namely, the volume (or mass) scattering β_s and absorption coefficient β_a. Thus,

$$\beta_e = \beta_s + \beta_a \quad . \tag{3}$$

Normally, molecules and particulates in the atmosphere scatter and absorb solar and infrared radiation. In the infrared window of 9 to 12 micrometers which is of interest in this report, the author is not too concerned with the scattering by gas molecules. In comparison with the magnitude of the scattering by aerosol and cloud particles, molecular scattering is entirely negligible in the infrared spectrum. In the solar spectrum, however, molecular and particulate scatterings are both important.

Returning to Eq. (1), note that in the absence of an external source the equation reduces to a form which, upon integration, gives one of the fundamental laws in radiation, that is, Beer's or Bouguer's law of transmission. The geometry is now fixed to avoid an arbitrary path length. Figures 1 and 2 depict such a geometry in two and three dimensions. The radiance becomes a function of optical path or depth τ, zenith angle θ, and azimuth angle ϕ. Moreover, the atmosphere has inadvertently been treated as being made up of many stratified layers, that is, a plane-parallel atmosphere with infinite horizontal extent. As a matter of fact, this is how the planetary atmosphere is being handled in the vast majority of publications on visible and infrared radiative transfer either in a clear or a cloudy medium. From the figure, Eq. (1) can be transformed into the following expression:

$$dI_\lambda(\tau;\ \theta,\ \phi) = -\beta_e I_\lambda(\tau;\ \theta,\ \phi)dz/\cos\theta + j_\lambda(\tau;\ \beta,\ \phi)\ dz/\cos\theta \quad , \tag{4}$$

from which we arrive at a form of the radiative transfer equation usually found in the literature, by setting

$$d\tau = -\beta_e dz \quad , \tag{5}$$

and $\mu = \cos\theta$; thus,

$$\mu \frac{dI_\lambda(\tau;\ \theta,\ \phi)}{d\tau} = I_\lambda(\tau;\ \theta,\ \phi) - J_\lambda(\tau;\ \theta,\ \phi) \quad . \tag{6}$$

where the source function $J_\lambda = j_\lambda/\beta_e$.

As it stands, the above differential equation can be solved analytically without having to know what the source J stands for. In the infrared region, a nonscattering, plane parallel atmosphere which is in local thermodynamic equilibrium may be considered. Thus, the source in this case is simply given by

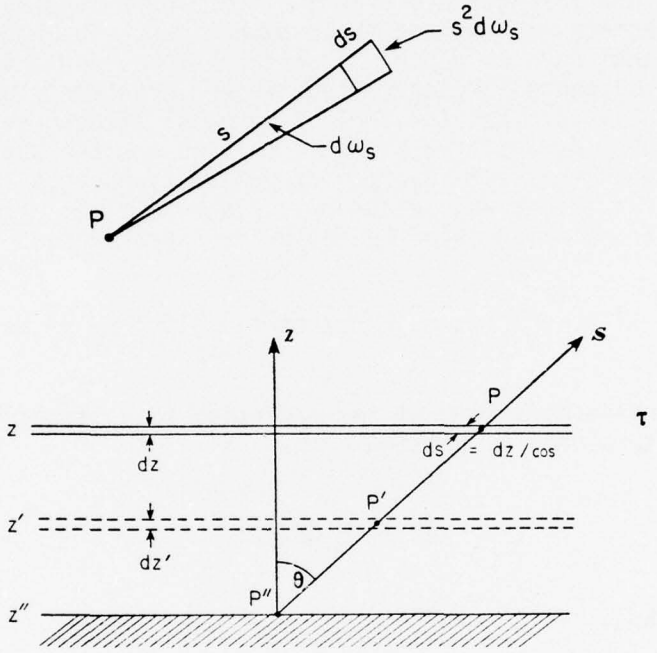

Figure 1. A plane-parellel atmosphere.

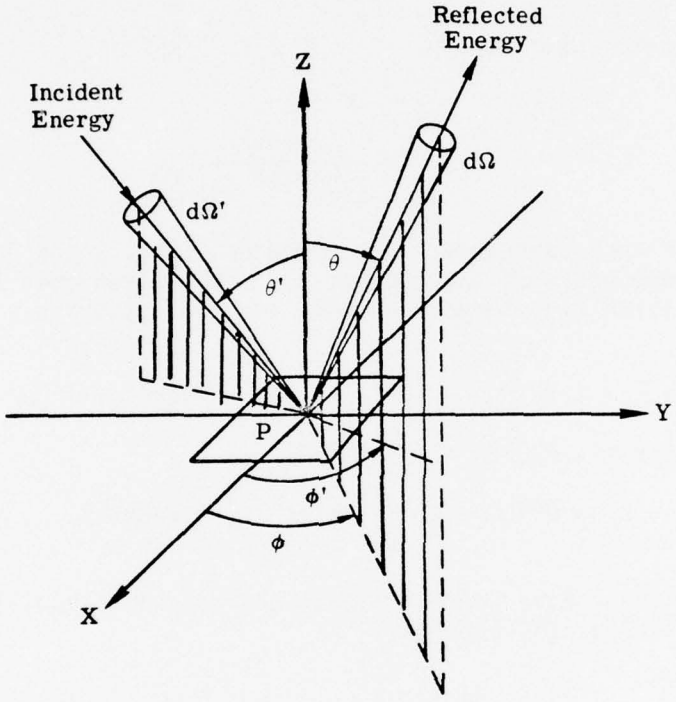

Figure 2. Spherical geometry of scattering.

$$J_\lambda(\tau;\ \theta,\ \phi) = B_\lambda(T) \quad , \tag{7}$$

where $B_\lambda(T)$ is the well-known Planck function. In the wavelength domain, it is given by

$$B_\lambda(T) = \frac{2hc^2}{\lambda^5(e^{hc/kt\lambda}-1)} \quad , \tag{8}$$

whereas in the wavenumber domain

$$B_\nu(T) = \frac{2h\nu^3c^2}{(e^{hc\nu/kT}-1)} \quad , \tag{9}$$

where h is the Planck constant, c the speed of light, k the Boltzmann constant, T the temperature of the medium, and ν the wavenumber (cm^{-1}). According to Rossini [4], these constants are, in cgs units,

$$\begin{aligned} 2hc^2 &= 1.191062 \times 10^{11} \text{ ergs sec}^{-1} \text{ cm}^{-2} \text{ sr}^{-1} \ \mu m^4, \\ hc/k &= 1.438786 \times 10^4 \ \mu m \ ^\circ K, \\ c &= 2.99792458 \times 10^{10} \text{ cm sec}^{-1} \text{ (in vacuum).} \end{aligned} \tag{10}$$

For a purely emissive atmosphere in local thermodynamic equilibrium, the radiative transfer Eq. (6) becomes

$$\mu \frac{dI_\lambda(\tau;\ \theta,\ \phi)}{d\tau} = I_\lambda(\tau;\ \theta,\ \phi) - B_\lambda(T) \quad , \tag{11}$$

Now the contribution to extinction comes solely from absorption. This equation holds for blackbody radiation and can be readily solved by introducing the integrating factor $e^{-t/\mu}$. In the retrieval of temperature profiles from the satellite vertical temperature profile radiometer (VTPR) data, Eq. (11) is solved in a reverse manner to determine the Planck function from which the atmospheric temperature is extracted. In theory, this equation governs the generation of infrared imagery in clear air.

The additional contribution to the source function due to multiple scattering is found for a scattering atmosphere.

$$J_\lambda(\tau;\ \theta,\ \phi) = \frac{\tilde{\omega}_o}{4\pi} \int_0^{\pi} \int_0^{2\pi} P_\lambda(\tau;\ \theta,\ \phi;\ \theta',\ \phi')\ I_\lambda(\tau;\ \theta',\ \phi') \sin\theta'\ d\theta' d\phi' . \tag{12}$$

It is this source function that complicates the solution of the radiative transfer equation. In the above equation, $p_\lambda(\tau;\ \theta,\ \phi;\ \theta',\ \phi')$ is the normalized phase function, representing the fraction of incident radiant energy scattered by a unit volume at a level τ in the direction of $(\theta,\ \phi)$ when that volume is illuminated from the direction $(\theta',\ \phi')$. In representing the scattering of polarized light, the intensity components can be described by the four Stoke's parameters. The phase function now consists of four-by-four elements and is called the phase matrix. The Stoke's parameters make it possible to determine the state of polarization, which is of great value in explaining many atmospheric optical phenomena but of little concern in the infrared spectral region where emission dominates.

To simplify Eq. (12), use $\mu(=\cos\theta)$ as the functional variable. Equation (6) then assumes the following form:

$$\mu \frac{dI_\lambda(\tau;\ \mu,\ \phi)}{d\tau} = I_\lambda(\tau;\ \mu,\ \phi) - \frac{\tilde{\omega}_o}{4\pi} \int_0^{2\pi} \int_{-1}^{+1} P_\lambda(\tau;\ \mu,\ \phi;\ \mu',\ \phi')\ I(\tau;\ \theta',\ \phi')\ d\mu'\ d\phi' \quad ; \tag{13}$$

where $\tilde{\omega}_o = \beta_s/\beta_e$ is the albedo for single scattering, a function of optical path.

Equation (13) is valid for solar radiation in the visible band. However, the sun's rays incident upon the plane-parallel atmosphere are generally taken to be coming in a parallel beam and, hence, are azimuthal-dependent. Solar radiation is different from thermal radiation in that the latter may be considered isotropic, and, hence, azimuthal-independent. A parallel beam of solar radiation incident upon the atmosphere or the earth in the direction $(-\mu_o,\phi_o)$ has an angular distribution expressible in terms of Dirac's delta function in the form

$$I_{inc}(\tau;\ \mu,\ \phi) = E_s(\tau)\ \ \delta(\mu - \mu_o)\ \ \delta(\phi - \phi_o)\ . \tag{14}$$

It is convenient to separate the direct solar radiation field from the diffuse radiation field in this analysis. Thus, the total spectral radiance or intensity may be written as

$$I_\lambda(\tau;\ \mu,\ \phi) = I_{inc}(\tau;\ \mu,\ \phi) + I_{dif}(\tau;\ \mu,\ \phi) \quad ; \tag{15}$$

which may then be substituted into Eq. (13) to yield

$$\mu \frac{dI_{dif}(\tau;\ \mu,\ \phi)}{d} = I_{dif}(\tau;\ \mu,\ \phi) - \frac{\tilde{\omega}_o}{4\pi} p(\tau;\ \mu,\ \phi;\ -\mu_o',\ \phi_o') E_s(\tau)$$

$$- \frac{\tilde{\omega}_o}{4\pi} \int_0^{2\pi} \int_{-1}^{+1} p(\tau;\ \mu,\ \phi;\ \mu',\ \phi')\ I_{dif}(\tau;\ \mu',\ \phi')\ d\mu' d\phi' \quad , \tag{16}$$

where $E_s(\tau) = \pi F e^{-\tau/\mu_o}$. In this equation, the wavelength subscript λ has been dropped since it is felt that no misunderstanding should arise by now as to the monochromatic nature of the radiative transfer equation as presently formulated. The subscript dif will also be dropped since only the diffuse radiation field will be dealt with. However, the solar term E_s, which is known as the reduced incident or direct radiation in the literature, must be included in the final accounting of reflected and transmitted radiation.

In theory, Eq. (16) is the governing equation for visible imagery. It applies to a scattering and absorptive atmosphere, whereas Eq. (11) applies to an absorptive and emissive one. An atmosphere which absorbs necessarily emits. The emission occurs at much longer wavelength or small wavenumber, the so-called long-wave radiation in meteorology. In a purely scattering medium, $\tilde{\omega}_o = 1$. In a purely absorptive and emissive one, $\tilde{\omega}_o = 0$. In general, in an atmopshere where scattering, absorption, and emission take place simultaneously, Eq. (11) is added to Eq. (16) to obtain

$$\mu \frac{dI(\tau;\ \mu,\ \phi)}{d\tau} = I(\tau;\ \mu,\ \phi) - (1 - \tilde{\omega}_o) B_\lambda[T(\tau)]$$

$$- \frac{\tilde{\omega}_o}{4} F e^{-\tau/\mu_o} p(\tau;\ \mu,\ \phi;\ -\mu_o',\ \phi_o')$$

$$- \frac{\tilde{\omega}_o}{4\pi} \int_0^{2\pi} \int_{-1}^{+1} p(\tau;\ \mu,\ \phi;\ \mu',\ \phi')\ I(\tau;\ \mu',\ \phi')\ d\mu' d\phi' \tag{17}$$

This radiative transfer equation, in its full ominous appearance, describes the monochromatic transfer of solar radiation in a vertically inhomogeneous atmosphere which is assumed to be in local thermodynamic equilibrium. This integro-differential equation is difficult to solve for the general case of multiple scattering; thus, numerical techniques are normally being employed. Since solar and thermal infrared spectra are in two distinct regions where overlapping can be ignored, solar and infrared radiation can be treated separately [5]; thus, in the infrared region the third term on the right side of Eq. (17) can be neglected and the following is left

$$\mu \frac{dI(\tau; \mu, \phi)}{d\tau} = I(\tau; \mu, \phi) - (1 - \tilde{\omega}_o) B_\nu[T(\tau)] - \frac{\tilde{\omega}_o}{4\pi} \int_0^{2\pi} \int_{-1}^{+1} p(\tau; \mu, \phi; \mu', \phi') I(\tau; \mu', \phi') d\mu' d\phi' \tag{18}$$

which is what is needed in the determination of the radiation properties of several cloud types. Owing to the isotropic radiation pattern emitted by the earth's surface, we may assume to a good approximation that the emergent radiation is independent of azimuth angles, thereby greatly improving the appearance of the phase function and hence the transfer equation. Moreover, if the choice is to work with relatively thin layers so that each layer becomes essentially homogeneous in its microstructure, then the single scattering albedo and the phase function are no longer functions of the optical path or, more appropriately, optical depth in view of the plane-parallel medium. In doing so, Eq. (18) is reduced to

$$\mu \frac{dI(\tau; \mu)}{d\tau} = I(\tau; \mu) - (1 - \tilde{\omega}_o) B_\nu[T(\tau)] - \frac{\tilde{\omega}_o}{2} \int_{-1}^{+1} p(\mu, \mu') I(\tau; \mu') d\mu' \tag{19}$$

where the phase function is given by

$$p(\mu, \mu') = \frac{1}{2\pi} \int_0^{2\pi} p(\mu, \phi; \mu', \phi') d\phi' \tag{20}$$

This is the form of the radiative transfer equation usually given in the literature for infrared radiation. The variable τ is also used to denote

the levels at which upward and downward radiation emerges. The emergent radiances thus illuminate two hemispheres; therefore, it would be convenient to separate the two hemispheres so that the emerging radiation can be resolved into an upwelling branch and a downwelling branch. In satellite work, interest lies in the former for this is what the infrared radiometer on board a satellite presumably "sees." Then, Eq. (19) may be decomposed into two equations.

Upward: $0 < \mu \leq 1$

$$\mu \frac{dI(\tau; +\mu)}{d\tau} = I(\tau; +\mu) - (1 - \tilde{\omega}_o) B_\nu[T(\tau)] - \frac{\tilde{\omega}_o}{2} \int_{-1}^{+2} p(+\mu, \pm\mu') I(\tau; \pm\mu') d\mu' \tag{21a}$$

Downward: $0 < \mu \leq 1$

$$\mu \frac{dI(\tau; -\mu)}{d\tau} = -I(\tau; -\mu) + (1 - \tilde{\omega}_o) B_\nu[T(\tau)] + \frac{\tilde{\omega}_o}{2} \int_{-1}^{+1} p(-\mu, \pm\mu') I(\tau; \pm\mu') d\mu' \tag{21b}$$

The scattering integrals in Eqs. (21a, b) are represented, respectively, by

$$\int_{-1}^{+1} p(+\mu, \pm\mu') I(\tau; \pm\mu') d\mu' = \int_{o}^{1} p(+\mu, +\mu') I(\tau; +\mu') d\mu' + \int_{o}^{1} p(+\mu, -\mu') I(\tau; -\mu') d\mu' \tag{22a}$$

$$\int_{-1}^{+1} p(-\mu, \pm\mu')\, I(\tau; \pm\mu')\, d\mu' = \int_{0}^{1} p(-\mu, +\mu')\, I(\tau; +\mu')\, d\mu'$$

$$+ \int_{0}^{1} p(-\mu, -\mu')\, I(\tau; -\mu')\, d\mu' \qquad (22b)$$

With the above expressions, the derivation of the radiative transfer equation for the infrared spectral region is complete. The solutions of Eqs. (21a, b) for the purpose of examining the optical properties of clouds in satellite applications will be presented in later sections.

EXTINCTION COEFFICIENTS AND PHASE FUNCTION

In the radiative transfer equation, there are several optical parameters that need be fixed, namely, the extinction, scattering, and absorption coefficients, β_e, β_s, and β_a, derivable from the so-called Mie parameters; the optical depth τ, obtainable directly from these coefficients, as demonstrated in Eq. (5); and the phase function which is usually made up of two scattering functions, Rayleigh and Mie. In infrared radiation where thermal radiation dominates almost completely (see, for example, Yamamoto et al. [6]), Rayleigh scattering by air molecules is generally neglected, although it can be easily computed. It may be included in the following manner:

$$p(\tau; \mu, \mu') = T(\tau)\, M(\mu, \mu') + [(1 - T(\tau)]\, R(\mu, \mu') \qquad (23)$$

where $T(\tau)$ is the turbidity factor defined by

$$T(\tau) = \tau_{s,m}/(\tau_{s,m} + \tau_{s,r}) \qquad (24)$$

where $\tau_{s,m}$ and $\tau_{s,r}$ represent, respectively, the optical depths due to Mie and Rayleigh scattering. In Eq. (23), $M(\mu, \mu')$ and $R(\mu, \mu')$ are the Mie and Rayleigh phase functions, respectively.

However, molecular absorption in the 9- to 12-micrometer window is not negligible. The most important absorber in the window is water vapor. As a result, the optical depth parameter has one component due to water vapor absorption in addition to the absorption by aerosol and/or cloud particles.

Since the underlying theory and the computational techniques for these parameters including atmospheric transmission have been discussed in some detail by Gomez [7], Gillespie and Petracca [8], and Gomez et al. [9] among others in published ECOM reports, this short section can serve as a footnote to them. As a matter of fact, the present work may also be looked upon as a continuation of their effort in target signature studies.

It should be pointed out that this laboratory has several computer programs for computing the Mie coefficients and the phase function for any given particle size distributions and complex refractive indices and for calculating high-resolution atmospheric transmission due to molecular absorption.

CLOUD MICROSTRUCTURE

No matter how elegant mathematical techniques may be in computing the Mie coefficients and in constructing the Mie phase function or scattering diagram, results from the solution of the radiative transfer equation will not be very meaningful if the particle data and the complex refractive indices used in computing them are questionable. Therefore, it is important to gain a little understanding of cloud physics.

Our planetary atmosphere is never free of aerosol particles, but it is free of cloud particles for only a small part of the globe, as a glance over the GOES visible or infrared imagery will readily show. Aerosol is a colloidal system in which the dispersed phase is composed of either fine solid or liquid particles and in which the dispersion medium is usually the air. There is no clear-cut upper limit to the size of particles comprising the dispersed phase in an aerosol, but as in all other colloidal systems, it is rather commonly set at 1 micrometer. Haze, most smokes, and some fogs and clouds may be regarded as aerosols. However, it is not good usage to apply the term to ordinary clouds whose droplets are so large as to rule out the usual concept of colloidal stability. It is poor usage to apply the term to the dispersed particles alone, and aerosol is a system of dispersed phase and dispersing medium taken together.

With the aerosol thus clarified, a cloud can now be defined. A cloud is a visible aggregate of minute water and/or ice particles in the atmosphere above the earth's surface. Cloud differs from fog only in that the latter is, by definition, in contact with the earth's surface. Clouds form in the free atmosphere as a result of condensation of water vapor in rising currents of air and hence by cooling or by the evaporation of the lowest stratum of fog. For condensation to take place at the point of saturation or a low degree of supersaturation in the atmosphere, condensation nuclei are required for the formation of water clouds, while ice nuclei are required for ice-crystal clouds. The

size of cloud droplets varies from one cloud type to another. Within any given cloud, there always exists a finite range of sizes. Generally, cloud droplets range between 1 and 100 micrometers in diameter, and hence are very much smaller than raindrops, usually of the order of 1 millimeter or greater.

There is a connection between aerosol and cloud particles, but the connection is limited only to those aerosol particles which are in the neighborhood of 0.1 micrometer or larger in diameter and which are hygroscopic in the case of water clouds or have the capacity for ice nucleation in the case of ice clouds. These aerosol particles which have the ability to serve as such nuclei are generally referred to as cloud condensation nuclei or ice nuclei. The rest of the aerosol particles that do not partake in the cloud- or fog-forming process can be classified as haze particles. Another phenomenon is what is often called the dry haze, the visible evidence of the existence of aerosol in the air, when atmospheric humidity is low, or damp haze when humidity is relatively high. In the latter case, these haze particles must be hygroscopic. Near or at saturation, they may then form mist.

Given a slight supersaturation of the order of perhaps 0.01%, some of these haze particles or cloud embryos may overcome the critical free energy point to grow to larger sizes. In a damp haze, there could be a few scattered droplets, but they are of insufficient number to appear as a cloud or fog. Figure 3 is known as the Köhler curve of droplet growth. The highest point in the curve is the critical point which designates the so-called critical supersaturation and the critical radius of a condensation nucleus. Thus, the critical point is the dividing line between what the cloud physicist refers to as the haze particles on the stable side and the cloud droplets on the unstable side. When a condensation nucleus, necessarily of a sufficient size and hygroscopicity, grows into a droplet, it may be said that the droplet has reached infinite dilution. For all practical purposes, a cloud droplet can be considered a pure water droplet.

The somewhat lengthy description of aerosol, haze, and cloud particles given above was taken from well-known cloud physics books [10,11,12] and the Glossary of Meteorology [13] in order to clarify that aerosol, haze, and cloud particles do not mean the same thing. In dealing with the aerosol particles, not all of which can properly be regarded as spherical particles, chemical composition should be of concern. In contrast, the haze particles and the cloud droplets can be treated as spherical particles. In the former, chemical composition is still important, while in the latter it can be disregarded. In optical property, calculations show that the extinction coefficient of a spherical particle 10 micrometers in diameter is about 30 times greater and that of a 5-micrometer particle about 10 times greater than that of a 1-micrometer particle in the 10-micrometer window without regard to their composition. When particles

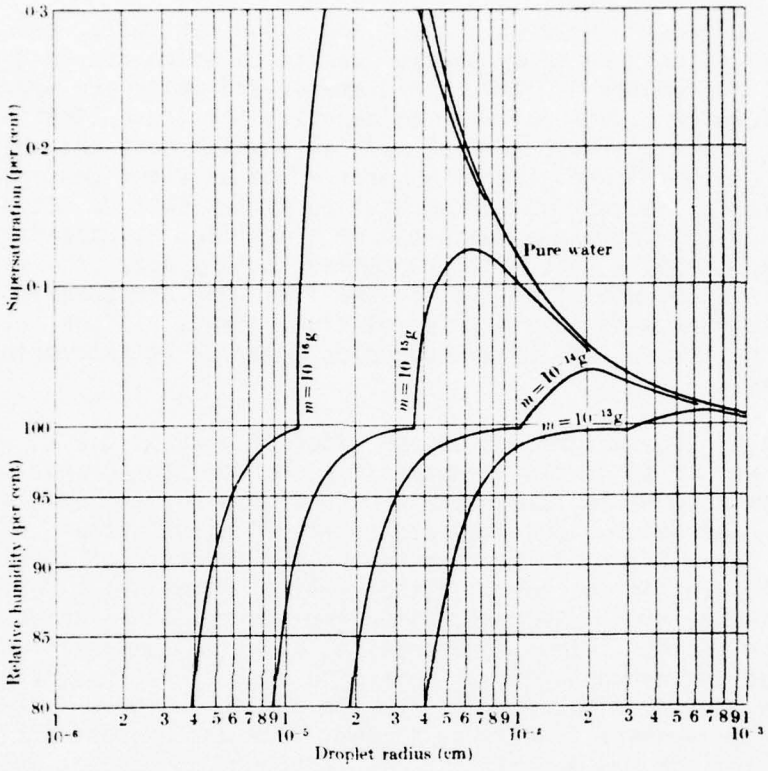

Figure 3. The equilibrium supersaturation as a function of droplet radius for solution droplets containing the indicated masses of sodium chloride. (From Mason, 1971)

range from 0.0001 to 0.1 micrometer in diameter, as are usually found in aerosol, their effect on transmission in the infrared window is quite negligible in comparison with the effect of cloud, haze, or even dust particles (in a sandstorm), as can be readily inferred from the figures depicting extinction and hence transmission in the ECOM report by Gomez et al. [9].

The study of cloud microstructure is only one facet of our interest in cloud physics which embraces not only the investigation of the condensation process and precipitation physics in clouds, but also radiative transfer, optical phenomena, electrical phenomena, and a wide variety of hydrodynamic and thermodynamic processes in clouds. In this section, we shall investigate the statistical features of cloud microphysics, ignoring its dynamic processes leading to the formation of the various cloud types and the techniques for sampling cloud droplets. Cloud and fog sampling has been in effect over 40 years. Innumerable droplet data have been collected. Yet, knowledge of the different types of cloud microstructure is still incomplete. The complexity arises from the fact that the microstructure is not only a function of cloud type but also of geographical location, position within the cloud, and time of cloud development. Great effort has been made in categorizing these clouds by means of different statistical parameters; however, success has generally been limited. Nevertheless, it may be of some interest to show how cloud microstructure varies with these factors. Figure 4, reproduced from Diem [14], shows the change as a function of cloud type. Figure 5 from Squires [15] shows the change with geographical location, Fig. 6 from Zaitsev [16] the change with height level, and Fig. 7 from Low [17] the change with time.

Of interest to the cloud physicist are such parameters as the size range, mean radius, mode radius, median radius, mean-volume radius, and liquid water content (LWC) which is expressed in unit of grams per cubic meter ($g\ m^{-3}$). Thus, particle size, distribution, concentration, thermodynamic phase, shape, and orientation constitute the so-called microstructure of clouds. Of no less importance, but so far not easily measurable, is the percentage of supersaturation attained in a cloud. In fact, it may be judged to be the most important. Given the supersaturation and the size distribution of condensation nuclei together with their hygroscopic property, these statistical parameters can be readily estimated (e.g., [18]). From condensation nucleus measurement, Twomey [19] estimated that supersaturation in natural clouds may be as low as 0.14% and as high as 1.1%, depending upon the ascent rate of the parcel of saturated air and the number of nuclei therein. Following the same approach, but employing a measuring technique, Low [20] showed that the supersaturation attained in the ordinary radiation-advection fogs varied from about 0.03% to about 0.10%, mainly due to radiation cooling.

Next, the liquid water content shall be mentioned briefly. The liquid water content can be calculated from the number concentration of cloud droplets (if sampled correctly) and measured with an instrument such as

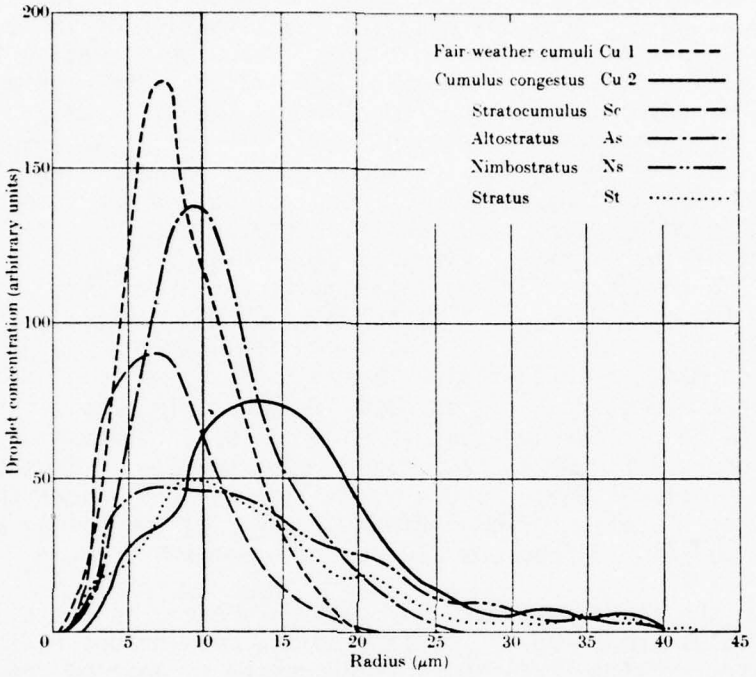

Figure 4. The mean droplet-size distribution of various cloud types. (From Diem, 1948)

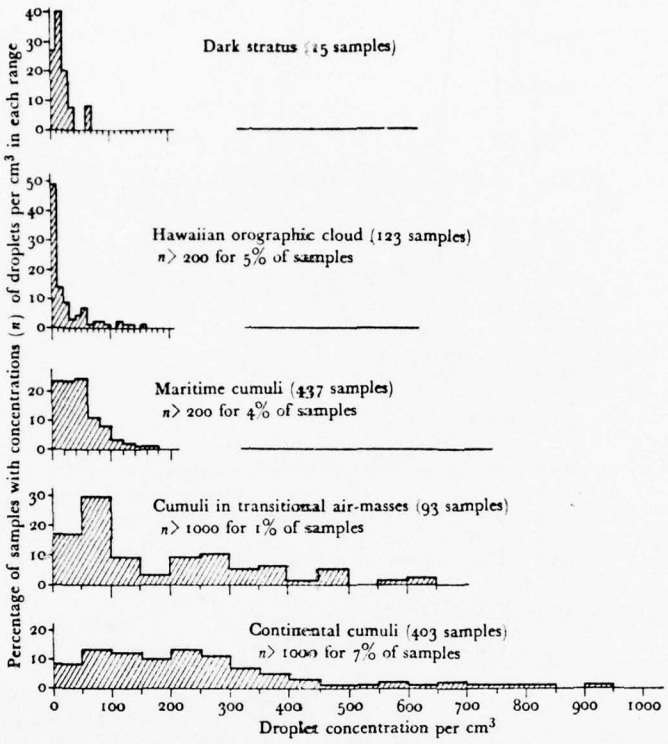

Figure 5. Histograms of the percentages of droplet samples taken, not all at the same geographical location, in each of five cloud types. (From Squires, 1958)

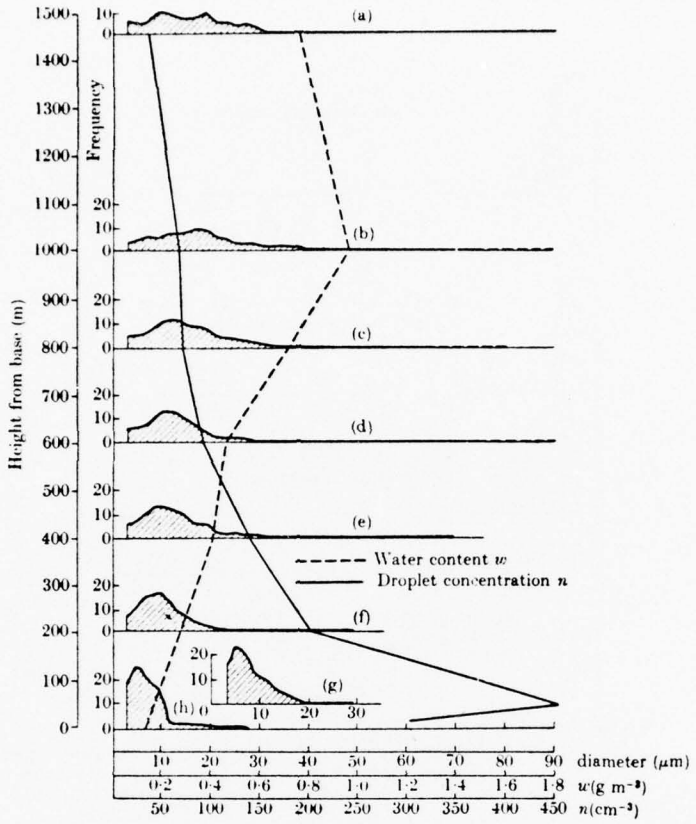

Figure 6. The droplet-size distribution, liquid water content, and droplet concentration as functions of height. (From Zaitsev, 1950)

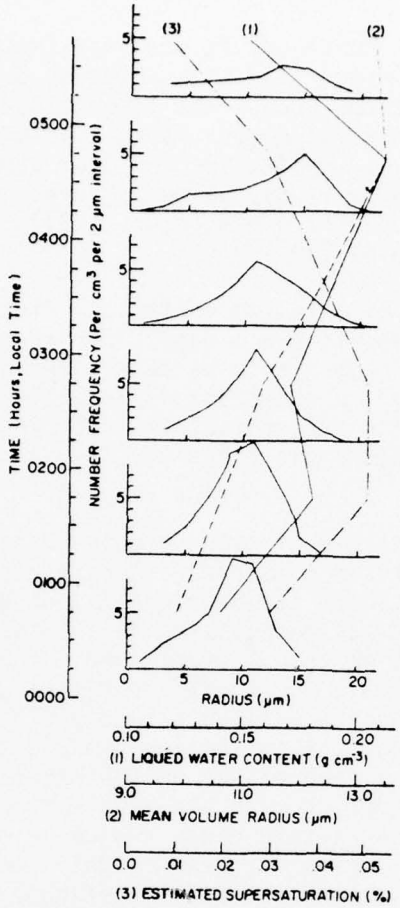

Figure 7. The droplet-size distribution, liquid-water content, mean volume radius, and supersaturation as functions of time. (From Low, 1975)

the hot-wire LWC meter. In clouds it can vary from about 0.15 g m^{-3} in a dry continental cumulus cloud [21] to as high as 3.9 g m^{-3} in a highly convective cumulus congestus [22]. The other cloud types apparently fall somewhere in between these extremes. As to the fogs, the microphysical data are not so extensive. Again, the fog microstructure depends upon the type and other factors; it may be wet or dry. Inland fogs may have an average value of about 0.17 g m^{-3} (e.g., [23]), and coastal fogs an average value of about 0.41 [20].

With the droplet data available, an analytical distribution or density function can be chosen to fit these data. For raindrop size distribution, the Marshall-Palmer [24] appears to be generally accepted. For cloud droplet size distribution, a number of distribution functions have been suggested, notably, Best's exponential distribution [25], the lognormal distribution [26], the gamma distribution [27], and the Khrgian-Mazin distribution [28].

Because of the complex nature of cloud droplet data, these data can fit a variety of standard or nonstandard density functions, depending upon where, in what type of cloud, at what level, and when they are collected. It would perhaps be somewhat pedantic to deliberately choose a more complicated distribution function than a simple one. In an exhaustive comparison among Best's, the lognormal, and their own distribution functions on the basis of approximately half a million stratocumulus cloud droplet samples, Khrgian and Mazin [29] noted that the lognormal distribution showed a slightly greater accuracy than either of the others. Borovikov [11] felt that the complexity of working with the lognormal distribution rendered it difficult to handle in certain cases and would perhaps more than offset the advantage gained in greater accuracy. Until more convincing evidence dictates otherwise, the author of the present paper shall choose the Khrgian-Mazin distribution function because of its greater simplicity. As such, the function is given by

$$n(r) = Ar^2 \exp(-br) \quad , \tag{25}$$

where $n(r)$ is the number of droplets per cm^3 in size r per unit radius interval, and A and b are constants. This distribution may be seen as a modified gamma distribution of two parameters, α and β, with α set to 2 and $\beta = 1/b$. In fact, when α is set to 0, the Marshall-Palmer distribution for raindrops obtains.

As a probability density function, the constant A in Eq. (25) becomes

$$A = b^3/2 \tag{26}$$

and the other statistical parameters calculated from the moment generating function of the gamma distribution are as follows:

Mean radius $r_m = 3/b$

Mode radius $r_d = 2/b$

Dispersion $\sigma^2 = 3/b^2$

Liquid water content in g m^{-3}

$$W = 9.30842\ N\ r_m^3 \times 10^{-6} \qquad (27)$$

where N is the total number of droplets per cm^3, and r_m is expressed in micrometers. Here, the density of a cloud droplet is assumed to be unity. However, this assumption cannot be conveniently made in the case of haze particles, as already noted.

With the distribution function thus fixed, attention is directed to the types of clouds to be dealt with. The principal types, with the exception of the cirrus, but not their variations, will be considered. There is an extreme paucity of cirrus data, and no less serious is the uncertainty about the scattering properties for the irregularly shaped ice crystals of the cirrus. In fact, any clouds whose tops reach well above the freezing level may contain ice crystals. Single scattering properties of these nonspherical ice crystals would be difficult to generate. The following table summarizes the statistics of the warm clouds which will be used in the present report:

CLOUD TYPES, TEMPERATURES, AND STATISTICAL PARAMETERS

Type	T (°C)	r_{min} (μm)	r_m	r_{max}	LWC (g m^{-3})	N	b	NA
St, Sc, and Ac	5	1	4-7	20	0.12-0.40	125-200	0.750	42.18750
Cumulus (continental)	1	2	5-9	25	0.20-0.50	75-170	0.600	18.36000
Cumulus (maritime)	3	2.5	8-12	30	0.40-0.80	50-85	0.375	2.24121
Cumulus (fairly strong)	0	3	10-15	40	0.60-1.50	25-65	0.300	0.87750

Note: Underlined numbers are being used as computer inputs.

Surface Temperature = 32°C

By scanning the microphysical data documented in the books, particularly Borovikov's, the author mentally averaged the numbers and then juggled them so as to come up with what he believed to be reasonable ranges for the middle to high clouds in midlatitude summer months. The cloud temperatures were obtained in the same manner by consulting the climatological tables (e.g., Upper-Air Climatology of the United States [30]). With these cloud parameters the radiative transfer equation can be solved and the optical properties and emergent radiances in the infrared window region can be determined.

SOLUTION OF THE RADIATIVE TRANSFER EQUATION

There are a number of techniques for solving the radiative transfer equation, completely or approximately. Among them are the so-called exact solution for pure Rayleigh scattering [31], the doubling method for a homogeneous medium [32,33,34], the iteration method [35,36,37], the discrete ordinate method [38], the spherical harmonics technique (e.g., [39]), the invariant imbedding method [40], and the Monte Carlo method [41]. These different methods have been reviewed by Yamamoto and Tanaka [42] and by Hansen and Travis [43].

A majority of the authors dealing with transfer problems are either astrophysicists or physicists. Generally, they are concerned with the stellar or solar radiation. Apparently, they were not interested in radiative transfer in the infrared spectral region until the successful orbiting of the TIROS series in early 1960 made infrared cloud imagery available to the meteorologists day and night. Even so, comparatively fewer papers have been published on this subject. Yamamoto et al. [6] seem to be among the earliest atmospheric physicists to deal seriously with the scattering, absorptive, and emissive properties of water clouds in the 10-micrometer infrared window, first by expanding the transmission, scattering, and emission functions into power series and then by iteration to obtain the final solution.

In a later paper, Yamamoto et al. [44] showed how to obtain integrated upwelling and downwelling radiation over a broad infrared band on the basis of the same scheme. Zdunkowski and Choronenko [45] employed a straightforward iterative technique to investigate the blackness of isolated clouds. Hunt [46] used the matrix operation method to solve the transfer equation in both visible and infrared spectral regions and presented numerous tables to depict the optical properties of both water and ice clouds; in doing so, he assumed the ice crystals to be spherical. In all these studies, clouds are assumed to be homogeneous in both temperature distribution and droplet number concentration.

Below, the equation will be solved by the Gauss-Seidel iteration method [47], following Herman and Browning [35]. Equations (21a) and (21b) are reformulated as follows:

$$\mu \frac{dI(\tau; +\mu)}{d\tau} = I(\tau; +\mu) - J(\tau; +\mu) \tag{21a}$$

$$\mu \frac{dI(\tau; -\mu)}{d\tau} = - I(\tau; -\mu) + J(\tau; -\mu) \tag{21b}$$

where

$$J(\tau; +\mu) = (1 - \tilde{\omega}_o)\, B[T(\tau)] + \frac{\tilde{\omega}_o}{2} \int_{-1}^{+1} p(+\mu; \pm\mu')\, I(\tau; \pm\mu')\, d\mu'$$

$$J(\tau; -\mu) = (1 - \tilde{\omega}_o)\, B[T(\tau)] + \frac{\tilde{\omega}_o}{2} \int_{-1}^{+1} p(-\mu; \pm\mu')\, I(\tau; \pm\mu')\, d\mu'$$

Note that the scattering integrals are given by Eqs. (22a) and (22b).

Figure 1 shows that the cloud may be sliced into N thin layers of equal geometric thickness, as in our case, or of equal optical thickness, from the top to the bottom in opposite direction to geometric height; thus, the upper boundary of the cloud is labeled n = 1, and the first layer n = 1 for n = 1, 2, 3, . . . N + 1 levels and n = 1, 2, 3, . . . N layers. For the present, the optical mass from space down to the upper boundary (i.e., n = 1) is taken to be nil; hence, the optical thickness at n = 1, $\tau_1 = 0$. Then, $\tau_2 = \tau_1 + \tau_2$,/$\tau_3 = \tau_1 + \tau_2 + \tau_3$, and so on for levels 1, 2, ... N + 1. With this in mind, multiply Eq. (21a) by the integrating factor, $e^{+t/\mu}$ and Eq. (21b) by the factor, $e^{-t/\mu}$, and then integrate the resulting expressions successively from τ_1 to τ_2, τ_2 to τ_3, and so on. The following iteration formulas are obtained:

$$I(\tau_n; +\mu) = I(\tau_{n+1}; +\mu)\, e^{-(\tau_{n+1}-\tau_n)/\mu} + \int_{\tau_n}^{\tau_{n+1}} J(t; +\mu)\, e^{-(t-\tau_n)/\mu} \frac{dt}{\mu} \tag{28a}$$

$$I(\tau_n; -\mu) = I(\tau_{n-1}; -\mu)\, e^{-(\tau_n-\tau_{n-1})/\mu} + \int_{\tau_{n-1}}^{\tau_n} J(t; -\mu)\, e^{-(\tau_n-t)/\mu} \frac{dt}{\mu} \tag{28b}$$

For relatively thin layers of the order of perhaps 20 to 50 meters thick, depending on the type of cloud studied, an arithmetic mean of the source function J may be taken. Now let $\overline{J}(\tau_n; \pm\mu)$ be the average source function at the top and bottom of the nth layer and $\Delta\tau_k = \tau_n - \tau_{n-1}$ where k varies with the specification of n. Equations (28a) and (28b) may then be put into a rather compact form as follows, upon integration:

$$I(\tau_n; \pm\mu) = I(\tau_{n\pm1}; \pm\mu)\, e^{-\Delta\tau_k/\mu} + \overline{J}(\tau_k; \pm\mu)\,(1 - e^{-\Delta\tau_k/\mu}) \quad , \tag{29}$$

where positive values of μ (i.e., $+\mu$, upwardgoing)

$$k = n \quad , \quad \text{and } 1 \leq n < N + 1 \quad ,$$

and for negative values of μ (i.e., $-\mu$, downwardgoing)

$$k = n - 1 \quad , \quad \text{and } 1 < n \leq N + 1 \quad .$$

In using these compact notations, however, it should be noted that $\overline{J}(\tau_n; +\mu)$ and $\overline{J}(\tau_n; -\mu)$ are taken to mean the average radiation emerging at the top of the nth layer and at the bottom of the (n - 1)th layer, respectively.

Following Dave [37], the trapezoidal rule of integration will be employed to handle the scattering integrals in 2-degree intervals, after having obtained the mean intensity of the layer. For the other term in the source function, an arithmetic mean of the temperatures at two adjacent levels is taken.

To start Eq. (29), it is assumed that there shall be no multiple scattering at the beginning level; that is,

$$I(\tau_n; +\mu) = I(\tau_{n+1}; +\mu)\, e^{-\Delta\tau_n/\mu} + [1 - \tilde{\omega}_o(\tau_n)]\, B[\overline{T}(\tau_n)]\,(1 - e^{-\Delta\tau_n/\mu}) \quad , \tag{30a}$$

$$I(\tau_n; -\mu) = I(\tau_{n-1}; -\mu)\, e^{-\Delta\tau_{n-1}/\mu} + [1 - \tilde{\omega}_o(\tau_{n-1})]\, B[\overline{T}(\tau_{n-1})]\,(1 - e^{-\Delta\tau_{n-1}/\mu}) \tag{30b}$$

At this point, it may be appropriate to introduce the boundary conditions, noting that radiative transfer is a two-point boundary value problem. It is the usual practice in the literature to assume, though not quite correctly, that in the infrared region there is no radiation incident on the top of the cloud. This assumption shall be adopted for the present; then

$$I(\tau_1; -\mu) = 0 \quad , \tag{31a}$$

where τ_1 refers to the optical thickness from space to the top of the cloud, which has already been assumed to be zero.

At the bottom of the cloud, if an isolated cloud is investigated as in the paper by Zdunkowski and Choronenko [45], the following would apply

$$I(\tau_b; +\mu) = 0 \tag{31b}$$

On the other hand, the ground surface may be the boundary in the case of a dry column below the cloud base; or a humid column together with ground radiation below the cloud base may be the boundary. In this present study, the former is adopted; thus,

$$I(\tau_b; +\mu) = B(T_g) \quad , \tag{31c}$$

where T_g is the temperature of the ground surface whose emissivity is assumed to be 1. Since this discussion is more centered in the optical properties of various cloud types at present, such as cloud emissivity and transmissivity, Eqs. (31a), (31b), and (31c) will be used.

Either the top level (i.e., n = 1) or the bottom level (i.e., n = N + 1) can be used as a start. For this discussion, begin with the top level and proceed to the base. During the downward excursion through each successive layer to the base, assume that there shall be no upward radiation. However, in going from the first to the second layer, the scattering due to downward emission, given by the second term on the right side of Eq. (22b) can no longer be neglected; it must be included in the computation. As the steps are traced upward through each succeeding layer, Eqs. (22a) and (22b) come into the picture. When the top level is reached, the first iteration has been completed. Equivalently, it may be said that the upward and downward radiation from first order scattering has been obtained. As the computation undergoes each successive iteration, each successively higher order scattering is taken into account. The iteration procedure terminates when for $m \geq 1$

$$I_{m+1}(\tau_{N+1}; -\mu)/I_m(\tau_{N+1}; -\mu) = \varepsilon \quad , \tag{32}$$

where ε has been set to 1.002 in this study.

So far the computation of the indispensable phase function has not been mentioned. Two separate computer programs have been obtained through the courtesy of NASA for the computation of the function. One is slightly more efficient than the other; however, the radiative transfer computer program used will accept the coefficients of the Legendre polynomials given by any phase function computations. Deirmendjian's book [48] is useful for a description of the computational technique for constructing the Mie scattering functions.

In concluding this section, it may be pointed out that the iteration scheme as outlined above will render it possible to calculate the transfer of infrared radiation in nonhomogeneous atmospheres or clouds. It is also possible to consider the variation of the distribution functions of molecules and/or particulates, although a large amount of computer time may be required.

NUMERICAL RESULTS

Numerical solutions of complex integro-differential equations invariably present the question of how reliable and accurate the numerical results are despite careful attention to the formulation of the algorithm and the convergence criterion. The best way to resolve the question is to compare the results with controlled or selected experiments. The authors of the present project hope to conduct such an experiment in the near future. A number of radiation results generated by various numerical techniques have already been published. Thus, from the comparisons of these methods, definitive information may be derived concerning the reliability of each method employed in the calculations.

A comparison of the intensity values given in graphical form by Yamamoto et al. [6] was more tractable because of their utilization of Deirmendjian's cumulus cloud model [49] whose phase functions were listed for several wavelengths in the infrared band. Therefore, it was possible first to check the phase function of this project for the same cloud model against that of Deirmendjian's (as later tabulated in his book [48]) and then to compare intensity values with Yamamoto's at the cloud top and other levels, utilizing their model cases. The intensity values carefully extracted from their graphs were found to lie well within 5% of ours in zenith angles from 0 up to about 60 degrees. Comparison with Hunt's cloud emissivity and transmissivity values [46], however, shows some differences because of the uncertainty involved in the values of phase functions. Nevertheless, for the two cases of water cloud at the 11-micrometer wavelength, emissivity and

transmissivity values of this project lie within 10% of his tabulated values using Hunt's cloud models. Therefore, it may be stated with confidence that the numerical outputs from this computer program employing the iteration method are at least comparable with those given by the adding method [46] and the technique of scattering and transmission functions [6].

As input data to the computer program, the values of the various cloud types presented in the table were used and the complex refractive indices for water sphere compiled by Irvine and Pollack [50] in the 9- to 12.5-micrometer band, which approximately corresponds to the bandwidth of infrared imagery in current use. Figure 8 shows the size distributions of three cloud models. The droplet size and the concentration scales for the stratus are at the top and on the right side of the figure, respectively. The stratus model is again used to demonstrate in Figure 9 how its volume extinction coefficient and the single scattering albedo vary with wavelength. This illustration implies that optically a cloud behaves differently at different frequencies. The same figure also shows the change of blackbody radiation with frequency. The optical properties of other cloud types will be different, but their variations with wavelength follow closely the curves as depicted in Figure 9. They will not be repeated for each case. Figure 10 is presented as an example of the change of cloud emissivity (or transmissivity) with wavelength and cloud depth. The cloud flux emissivity is usually defined by

$$e_\lambda(\tau) = 2\int_0^1 I_\lambda(\tau;\mu)\,\mu d\mu / B_\lambda(T_c) \tag{33}$$

whereas from a satellite point of view the upwelling cloud emissivity may be expressed by

$$\varepsilon_\lambda = I_\lambda(0;1)/B_\lambda(T_c) \quad , \tag{34}$$

where T_c is the cloud temperature $B_\lambda(T_c)$ its blackbody intensity, and $I_\lambda(0,1)$ the upwelling radiance at the cloud top. A similar expression holds for cloud transmissivity, except that the cloud temperature is now replaced by the Planck function of the surface temperature and the assumption is made that there is no cloud emission.

Since the present interest is in infrared imagery, only the 11.5-micrometer window will be investigated, to conserve computer time. The 11.5-micrometer window lies approximately in the middle of the frequency response curve of infrared imagery. Figure 11 shows how the emissivity of each cloud model varies with cloud depth. Ordinarily, infrared imagery at or near the subsatellite point is of more importance in the determination of cloud-top height since such imagery enables the determination to be made

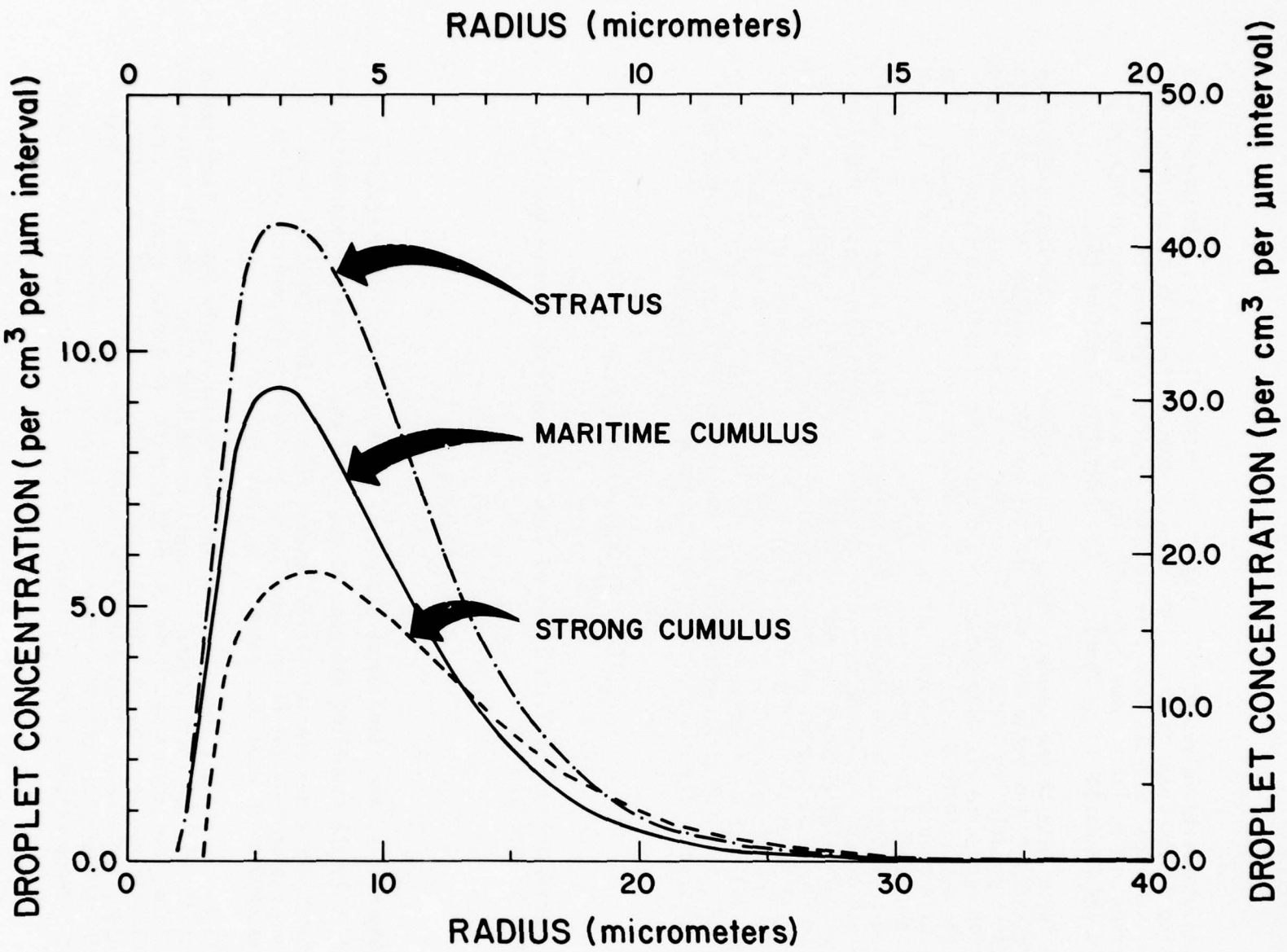

Figure 8. The droplet-size distributions of three cloud models. The scales at the top and on the right-hand side of the figure apply to the stratus only.

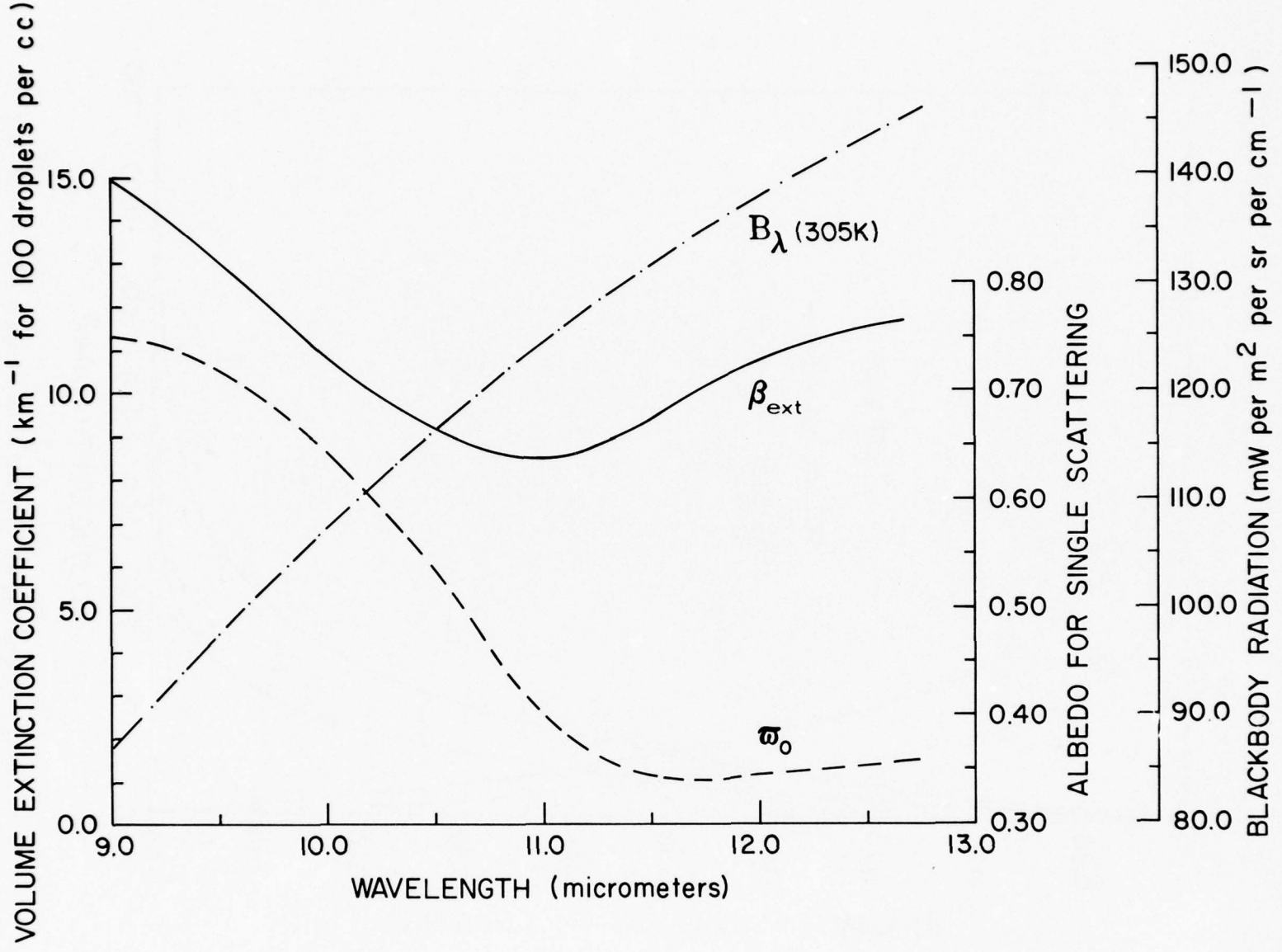

Figure 9. Typical variations of the volume scattering coefficient β_{ext}, the albedo for single scattering ϖ_0, the Planck function $B_\lambda(T)$ as a function of wavelength.

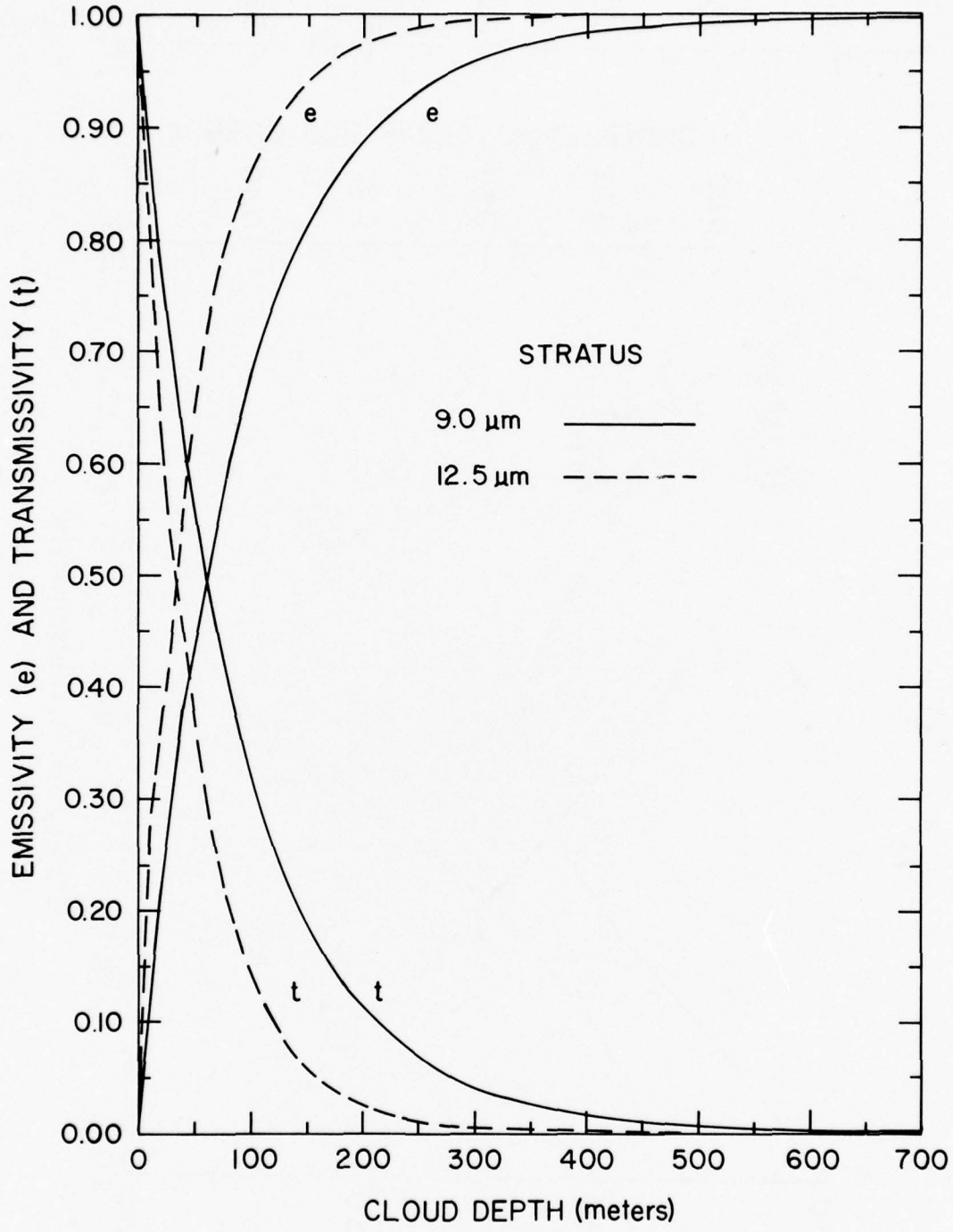

Figure 10. Transmissivity and emissivity of the stratus at two wavelengths as a function of cloud depth.

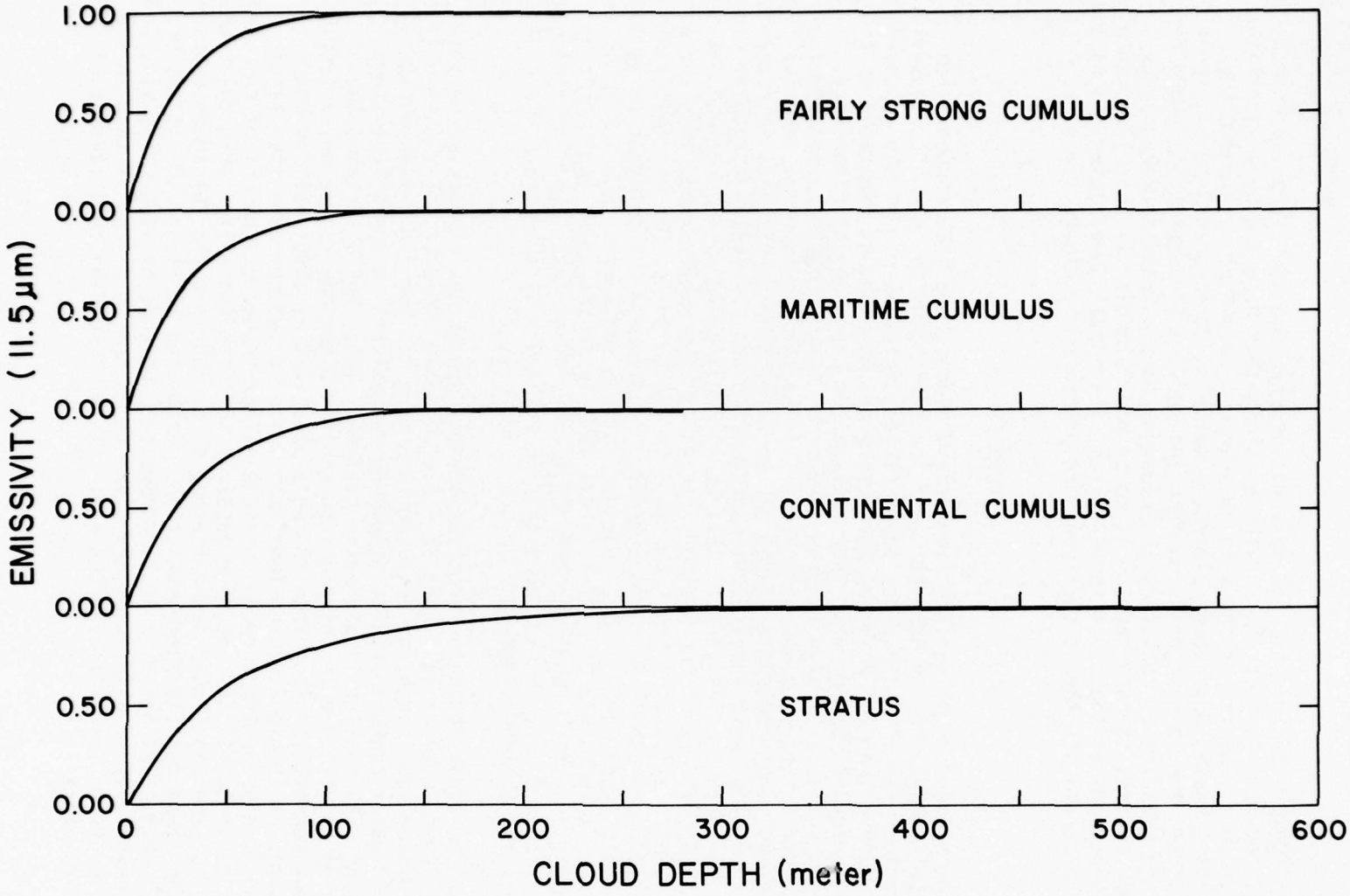

Figure 11. The emissivities of four cloud models at the 11.5-μm wavelength as a function of cloud depth.

with greater confidence. For this reason, Figure 12 depicts the normal upwelling radiation at the zenith, as presumably observed by a satellite radiometer. The insert shows an enlargement of the segment where the stratus emission approaches blackbody emission at about 650 meters above the cloud base when no emission from the surface is considered. When the surface emission is included, the cloud appears to radiate more energy at 650 meters, thereby causing it to become "blacker" at that level than the blackbody at the cloud temperature. The normal upwardgoing intensities at the zenith of other cloud types are presented in Figure 13.

DISCUSSION

In the present investigation, four cloud models have been chosen which are believed to be representative of the four cloud types. After experimentation with the stratus cloud of various thicknesses, it was discovered that, given the microphysical parameters of the cloud as tabulated in the table, no thickness greater than 1 kilometer needed to be considered. Moreover, the level at which the same cloud approaches the property of a blackbody varies with wavelengths, as can be readily inferred from the variation with wavelength of the volume extinction coefficient in Figure 9. The same cloud will appear the "blackest" in the 11- to 13-micrometer window region, which implies that the thickness required for it to radiate like a blackbody will be at the minimum. In fact, as shown by Hunt [46], for τ = 100, the emissivity of the same cloud is 0.8980 in the 3.8-micrometer window, but 0.9984 in the 11-micrometer window. To examine the internal radiation in detail, the cloud has been divided into 50 sublayers. However, this is not necessary in practice if interest is only in the upwelling radiation emerging from the cloud top. The test runs reveal that upwelling radiances vary within 0.2% by employing either 10 sublayers of 100 m each or 50 of 20 m each for a cloud layer.

Figure 10 again indicates that the stratus approaches blackbody radiation at a lower level at 12.5 than at 9 micrometers. However, at the same 11.5-micrometer wavelength, as depicted in Figure 11, the cloud with greater liquid water content attains blackbody radiation at a lower level than the one with smaller liquid water content. Thus, while it takes the stratus about 550 m in thickness to achieve blackbody radiation, a fairly strong convective cloud requires only about 220 m, about half as much. In terms of liquid water content, the latter cloud contains five times as much water as the former. Because of the tremendous amount of computer time required, it has not been possible to establish a tractable relationship between the liquid water content of a cloud and the thickness required of the cloud for blackbody radiation. Returning to Figure 10, it may be noted that at either 9 or 12.5 micrometers the sums of flux emissivity and transmissivity at all depths are close to unity; this implies that in the 10-micrometer infrared band there is little or no flux reflectivity of concern since

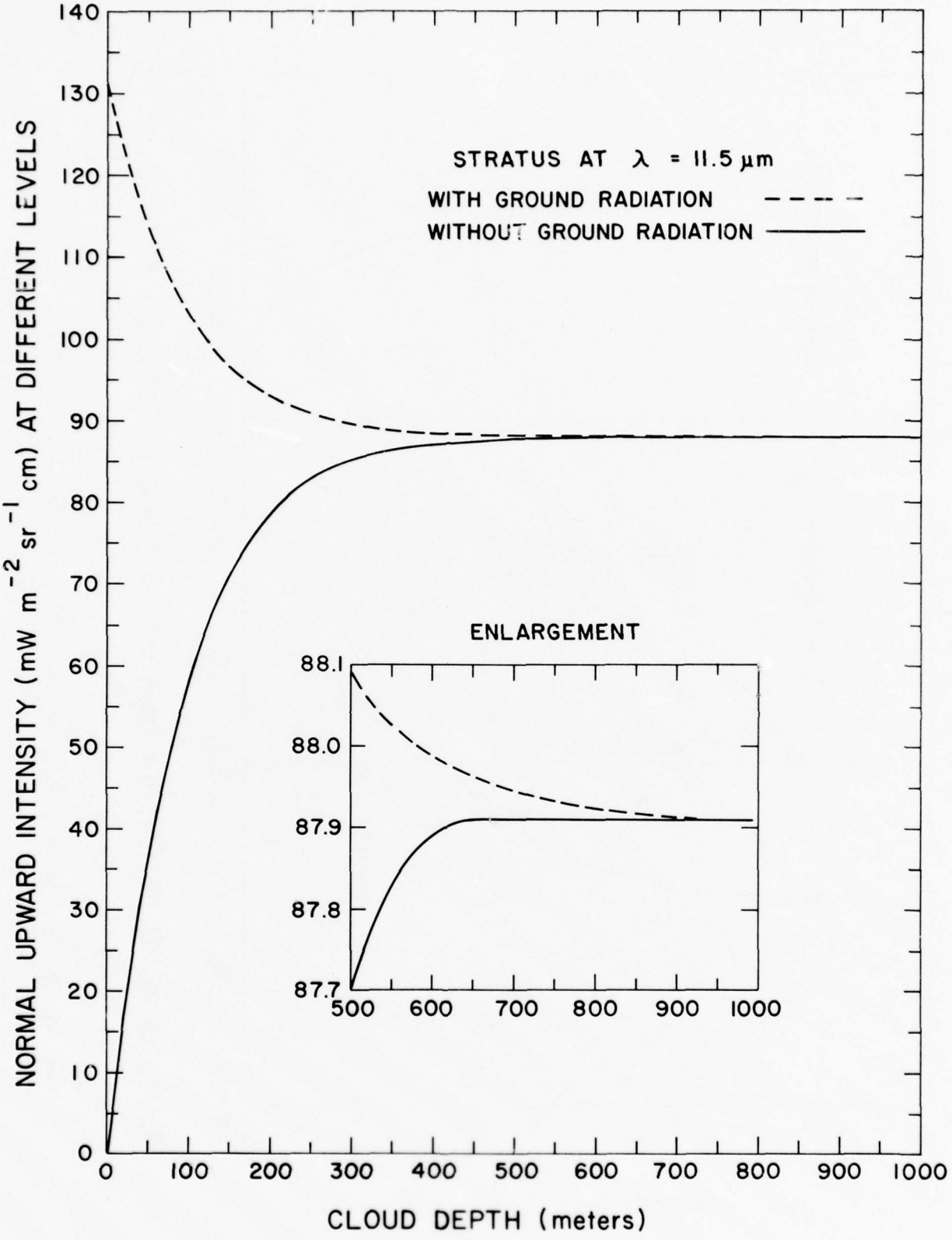

Figure 12. Upwelling radiation at the zenith at the 11.5-μm wavelength as a function of cloud depth.

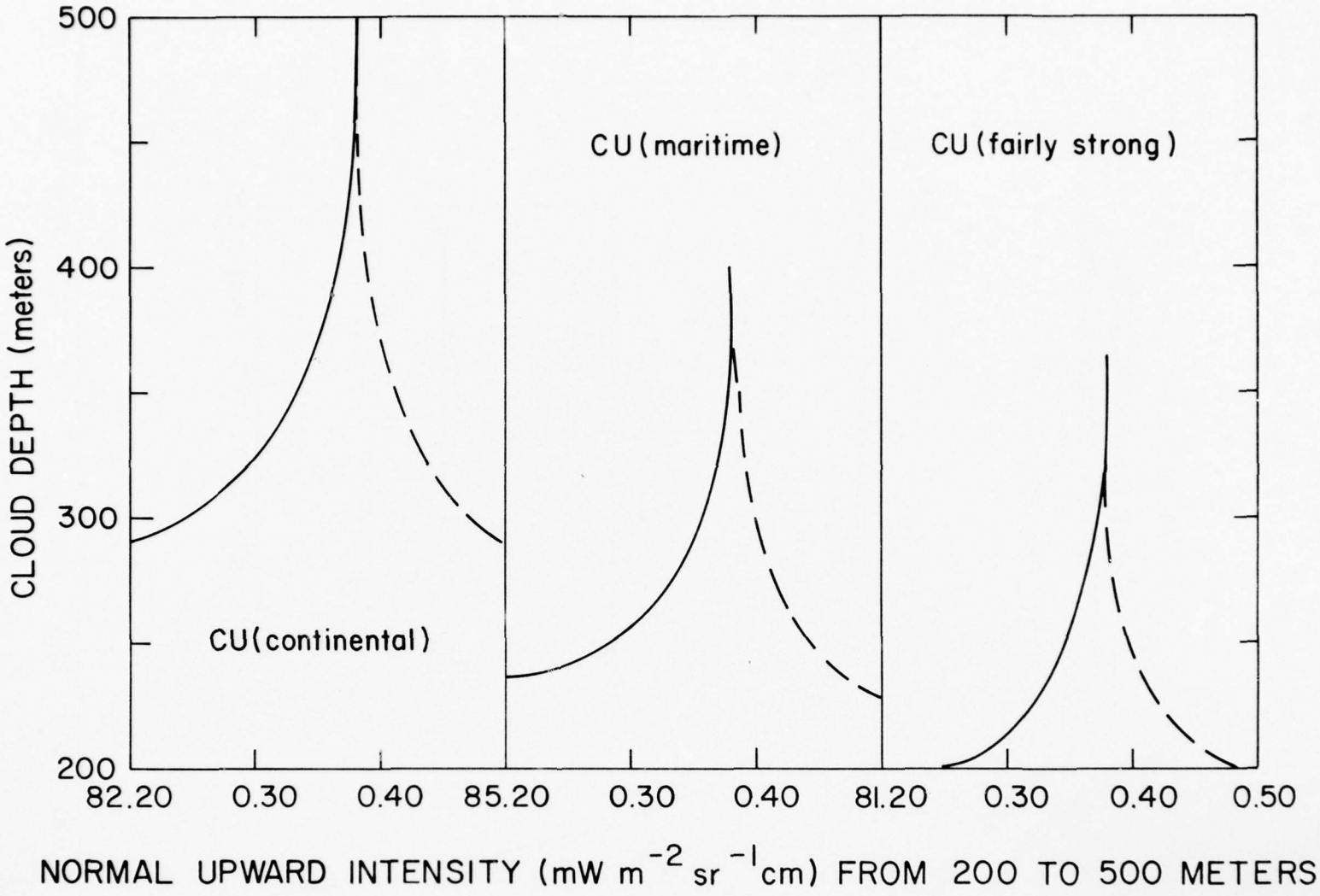

Figure 13. Upwelling radiation at the zenith at the 11.5-μm wavelength as a function of cloud depth.

$$t + e + r = 1 \quad , \tag{35}$$

where r is the reflectivity by the warm clouds.

When a cloud reaches a thickness such that it radiates almost like a blackbody, the upwelling radiation coming from the cloud top becomes very nearly isotropic, except towards the limbs. As was also found in our calculations, Zdunkowski and Choronenko [45] showed isotropic radiation at the cloud top for the case of an isolated cloud (i.e., without considering surface emission) and Yamamoto et al. [6] for the cases of nonisolated clouds (i.e., with surface radiation considered). Since infrared imagery is gray-scale contours of cloud-top intensities (i.e., radiances), the emergent radiation at or near the zenith is of particular interest, as already noted. In Figures 12 and 13, attention is directed toward the intersections of the solid and dashed lines. Although only the upwelling radiation has been displayed at the zenith for each case, it may be mentioned that up to 60 to 70 degrees the intersections are located at the same level for the same cloud model as a result of being isotropic. When there is no surface radiation, the solid curve approaches a straight line (i.e., blackbody radiation) at a level somewhat lower than that of the intersection. This is more prominent in the stratus model. As the liquid water content or the number of larger droplets increases, the effect of surface emission diminishes. The isolated stratus reaches blackbody radiation at about 660 m from its base, a continental cumulus at about 450 m, a maritime cumulus at about 370 m, and a fairly strong cumulus at about 330 m. In contrast, when surface radiation is present, the intersections, beyond which the cloud will radiate as a blackbody at its own temperature, are located, respectively, at about 940 m, 500 m, 390 m, and 330 m. Only in the last case, the solid and dashed lines meet at nearly the same level or depth, indicating that surface radiation has little effect on the level at which a heavily water-laden cloud attains blackbody radiation, whether in isolation or not.

What has just been discussed appears to be in conflict with the results described in Figure 11 with respect to cloud emissivity. It should be pointed out here that this inconsistency depends upon the application of the concept of emissivity. The conventional concept of emissivity is defined on the basis of radiation flux, expressed by Eq. (33). But from the point of view of satellite radiometer measures, the emissivity value should be given by Eq. (34). Thus, it is important that cloud emissivity be examined carefully in conjunction with satellite applications. The cloud cases investigated here show that the stratus reaches a depth of about 940 m (in theory) instead of 540 m before it becomes a blackbody from radiometric requirements. The continental cumulus must attain about 500 m instead of 280 m, the maritime cumulus about 390 m instead of 240 m, and the fairly strong convective cloud about 330 m instead of 220 m.

Of course, no cloud is ever isolated, nor is any cloud, except the fogs, ever in immediate contact with the ground surface without some intervening water vapor and temperature distributions, as are assumed in our present investigation as well as in the studies by Yamamoto et al. [6], Zdunkowski and Choronenko [45], and Hunt [46]. Nevertheless, the calculations presented here concerning the gross optical properties of clouds are by no means invalid, but rather represent a first step toward a better understanding and a more detailed examination of radiative transfer in clouds as is applicable to satellite problems.

CONCLUSIONS AND RECOMMENDATIONS

Thicknesses or depths required for blackbody radiation have been specified for the cloud types studied. Below these depths, the clouds will appear warmer than they actually are, as evident in Figure 13. When the cloud temperature is known, it appears possible to deduce the surface temperature in the absence of water vapor below the cloud base.

For satellite applications in which upwelling radiance (i.e., intensity) is measured, the conventional concept of emissivity can no longer be applicable. Instead, emissivity calculated on the basis of upwelling radiance should be introduced, thus making it appropriate for a proper interpretation of cloud-top temperatures. Note, however, the greater the amount of liquid water is in a cloud, the less is the difference between the two.

Reflectivity by warm clouds in the 10-micrometer infrared band is normally negligible.

The optical properties of a cloud are functions of wavelength, as also noted by other authors. The cloud appears more "black" in the neighborhood of the 11- to 13-micrometer window than in any other infrared windows.

The liquid water content of a cloud is an important microphysical parameter in relating directly to the degree of blackbody radiation. It requires further investigation to establish a functional relationship between the liquid water content of the cloud and the associated thickness for blackbody radiation.

During the next project, the computer program, which is now capable of solving the radiative transfer equation for an inhomogeneous cloudy atmosphere in the absence of water vapor absorption, will be modified to include such absorption both below and above the cloud as well as the frequency response function of the satellite radiometer in current use. In so doing, it will be possible to compare theoretical radiance values with those observed values from satellite data streams when the radiometer's field of view is partly or completely covered by clouds.

REFERENCES

1. Chandrasekhar, S., 1960, Radiative Transfer, Dover Publications, New York, NY.

2. Goody, R. M., 1964, Atmospheric Radiation: I. Theoretical Basis, Clarendon Press, Oxford, CT.

3. Kondratyev, K. Ya., 1969, Radiation in the Atmosphere, Academic Press, New York, NY.

4. Rossini, F. D., 1974, Fundamental Measures and Constants for Signs and Technology, Chemical Rubber Company Press, Cleveland, OH.

5. List, R. J., 1951, Smithsonian Meteorological Tables, Smithsonian Institution, Washington, DC.

6. Yamamoto, G., M. Tanaka, and K. Kamitani, 1966, "Radiative Transfer in Water Clouds in the 10-micron Window Region," J. Atmos. Sci., 23, 205.

7. Gomez, R. B., 1972, "Atmospheric Effects for Ground Target Signature Modeling: 1. Atmospheric Transmission at 1.06 Micrometer," ECOM-5445, Atmospheric Sciences Laboratory, White Sands Missile Range, NM.

8. Gillespie, J. B. and C. Petracca, 1974, "Atmospheric Effects for Ground Target Signature Modeling: II. Discussion and Application of a Generalized Molecular Absorption Model," ECOM-5531, Atmospheric Sciences Laboratory, White Sands Missile Range, NM.

9. Gomez, R. B., C. Petracca, C. Querfeld, and G. B. Hoidale, 1975, "Atmospheric Effects for Ground Target Signature Modeling: III. Discussion and Application of the ASL Scattering Model," ECOM-5558, Atmospheric Sciences Laboratory, White Sands Missile Range, NM.

10. Fletcher, N. H., 1962, The Physics of Rainclouds, Cambridge University Press, Cambridge, England.

11. Borovikov, A. M. and A. Kh. Khrgian, 1963, Cloud Physics, Israel Program for Scientific Translations, Jerusalem.

12. Mason, B. J., 1971, The Physics of Clouds, Clarendon Press, Oxford, CT.

13. Huschke, R. E., 1959, Glossary of Meteorology, Am. Meteorol. Soc., Boston, MA.

14. Diem, M., 1948, "Messungen der Grösse von Wolkenelementen, II," Meteorol. Res., 1, 261. (from Mason)

15. Squires, P., 1958, "The Microstructure and Colloidal Stability of Warm Clouds: I. The Relation Between Structure and Stability," Tellus, 10, 256.

16. Zaitsev, V. A., 1950, "Liquid Water Content and Distribution of Drops in Cumulus Clouds," Trudy Glavnoi Geofiz. Obs., 19, 12. (from Mason)

17. Low. R. D. H., 1975, "Microphysical Evolution of Fog," J. Recher. Atmos., 2, 23.

18. Howell, W. E., 1949, "The Growth of Cloud Drops in Uniformly Cooled Air, J. Meteorol., 6, 134.

19. Twomey, S., 1959, "The Nuclei of Natural Cloud Formation: II. The Supersaturation in Natural Clouds and the Variation of Cloud Droplet Concentration," Geofis. Bura. Appl., 43, 243.

20. Low., R. D. H., 1975, "Microphysical and Meteorological Measurements Fog Supersaturation," Tellus, 27, 507.

21. Kazas, V. I., 1963, "The Use of a Continuous Photoelectric Device for Studying the Microstructure of Clouds from an Aircraft," Izv. Akad. Nauk SSSR Ser. Geofiz., 5, 494 (from Mason)

22. Weickmann, H. K. and H. J. aufm Kampe, 1953, "Physical Properties of Cumulus Clouds," J. Meteorol., 10, 204.

23. Jiusto, J. E., 1964, "*Project FOG DROPS*," Report RM-1788-P-4, Cornell Aeronautical Laboratory, Buffalo, NY.

24. Marshall, J. S. and W. McK. Palmer, 1948, "The Distribution of Raindrops with Size," J. Meteorol., 5, 165.

25. Best, A. C., 1951, "Drop-Size Distribution in Cloud and Fog," Quart. J. Roy Meteorol. Soc., 76, 16.

26. Levin, L. M., 1954, "Distribution Function of Cloud and Raindrops by Sizes," Dokl. Akad. Nauk SSSR, 94, 1045. (translation)

27. Levin, L. M., 1958, "Functions to Represent Drop Size Distributions in Clouds: The Optical Density of Clouds," Izv. Geofiz. Ser., 10, 1211. (translation)

28. Khrgian, A. Kh. and I. P. Mazin, 1952, "The Size Distribution of Droplets in Clouds," Trudy TsAO, 7, 56. (translation)

29. Khrgian, A. Kh. and I. P. Mazin, 1956, "Analysis of Methods of the Characterization of Distribution Spectra of Cloud Droplets," Trudy TsAO., 17. (from Borovikov and Khrgian)

30. Office of Climatology, 1957, Upper-Air Climatology of the United States: Part I. Averages for Isobaric Surfaces, USWB, Washington, DC.

31. Coulson, K. L., J. V. Dave, and Z. Sekera, 1960, "Tables Related to Radiation Emerging from a Planetary Atmosphere with Rayleigh Scattering," University of California Press, Berkeley, CA.

32. Van de Hulst, H. C., 1963, "A New Look at Multiple Scattering," NASA Inst. for Space Studies, New York, NY.

33. Hansen, J. E., 1969, "Radiative Transfer by Doubling Very Thin Layers," Astrophys. J., 155, 565-573.

34. Hunt, C. E. and I. P. Grant, 1969, "Discrete Space Theory of Radiative Transfer and its Application to Problems in Planetary Atmospheres," J. Atmospheric Sci., 26, 963.

35. Herman, B. M. and S. R. Browning, 1965, "A Numerical Solution to the Equation of Radiative Transfer," J. Atmospheric Sci., 22, 559.

36. Irvine, W. M., 1968, "Multiple Scattering by Large Particles: II. Optically Thick Layers," Astrophys. J., 152, 823-834.

37. Dave, J. V., 1972, "Development of Diagrams for Computing Characteristics of Ultraviolet Radiation-Scaler Case," Contract NAS 5-21680, IBM Scientific Center, Palo Alto, CA.

38. Liou, K. N., 1973, "A Numerical Experiment on Chandrasekhar's Discrete Ordinate Method for Radiative Transfer: Application to Cloudy and Hazy Atmosphere," J. Atmospheric Sci., 30, 1303.

39. Canosa, J. and H. R. Penafiel, 1973, "A Direct Solution of the Radiation Transfer Equation: Application to Rayleigh and Mie Atmospheres," J. Quant. Spect. Rad. Transf., 13, 21.

40. Bellman, R. and R. Kalaba, 1956, "On the Principle of Invariant Imbedding and Propagation of Through Inhomogeneous Media, Proc. Natl. Acad. Sci., 42, 629.

41. Collins, D. G. and M. B. Wells, 1965, "Monte Carlo Codes for Study of Light Transport in the Atmosphere: Vol. I. Description of Codes, Vol. II. Utilization," ECOM-00240-F(I) and ECOM-00240-F(II), US Army Electronics Command, Fort Monmouth, NJ.

42. Yamamoto, G. and M. Tanaka, 1974, "Radiative Transfer of Visible Radiation in the Turbid Atmospheres," Proc. UCLA International Conf. on Radiation and Remote Probing of the Atmosphere, 1973.

43. Hansen, J. E. and L. D. Travis, 1974, "Light Scattering in Planetary Atmospheres," Goddard Institute of Space Studies, New York, NY.

44. Yamamoto, G., M. Tanaka, and S. Asano, 1970, "Radiative Transfer in Water Clouds in the Infra-red Region," J, Atmospheric Sci., 27, 282.

45. Zdunkowski, W. G. and I. Chornonenko, 1969, "Incomplete Blackness of Clouds in the Infrared Spectrum," Beitr. Atmos. Phys., 42, 206.

46. Hunt, G. E., 1973, "Radiative Properties of Terrestrial Clouds at Visible and Infrared," Quart. J. Roy. Meteorol. Soc., 99, 346.

47. James, M. L., G. M. Smith, and J. C. Wolford, 1967, Applied Numerical Methods, International Textbook, Scranton, PA.

48. Deirmendjian, D., 1969, Electromagnetic Scattering on Spherical Polydisperions, Elsevier, NY.

49. Deirmendjian, D., 1964, "Scattering and Polarization of Water Clouds and Hazes in the Visible and Infrared," Appl. Opt., 3, 187.

50. Irvine, W. M. and J. B. Pollack, 1968, "Infrared Optical Properties of Water and Ice Spheres," Icarus, 8, 324.

ATMOSPHERIC SCIENCES RESEARCH PAPERS

1. Lindberg, J.D., "An Improvement to a Method for Measuring the Absorption Coefficient of Atmospheric Dust and other Strongly Absorbing Powders," ECOM-5565, July 1975.
2. Avara, Elton, P., "Mesoscale Wind Shears Derived from Thermal Winds," ECOM-5566, July 1975.
3. Gomez, Richard B. and Joseph H. Pierluissi, "Incomplete Gamma Function Approximation for King's Strong-Line Transmittance Model," ECOM-5567, July 1975.
4. Blanco, A.J. and B.F. Engebos, "Ballistic Wind Weighting Functions for Tank Projectiles," ECOM-5568, August 1975.
5. Taylor, Fredrick J., Jack Smith, and Thomas H. Pries, "Crosswind Measurements through Pattern Recognition Techniques," ECOM-5569, July 1975.
6. Walters, D.L., "Crosswind Weighting Functions for Direct-Fire Projectiles," ECOM-5570, August 1975.
7. Duncan, Louis D., "An Improved Algorithm for the Iterated Minimal Information Solution for Remote Sounding of Temperature," ECOM-5571, August 1975.
8. Robbiani, Raymond L., "Tactical Field Demonstration of Mobile Weather Radar Set AN/TPS-41 at Fort Rucker, Alabama," ECOM-5572, August 1975.
9. Miers, B., G. Blackman, D. Langer, and N. Lorimier, "Analysis of SMS/GOES Film Data," ECOM-5573, September 1975.
10. Manquero, Carlos, Louis Duncan, and Rufus Bruce, "An Indication from Satellite Measurements of Atmospheric CO_2 Variability," ECOM-5574, September 1975.
11. Petracca, Carmine and James D. Lindberg, "Installation and Operation of an Atmospheric Particulate Collector," ECOM-5575, September 1975.
12. Avara, Elton P. and George Alexander, "Empirical Investigation of Three Iterative Methods for Inverting the Radiative Transfer Equation," ECOM-5576, October 1975.
13. Alexander, George D., "A Digital Data Acquisition Interface for the SMS Direct Readout Ground Station—Concept and Preliminary Design," ECOM-5577, October 1975.
14. Cantor, Israel, "Enhancement of Point Source Thermal Radiation Under Clouds in a Nonattenuating Medium," ECOM-5578, October 1975.
15. Norton, Colburn and Glenn Hoidale, "The Diurnal Variation of Mixing Height by Month over White Sands Missile Range, NM," ECOM-5579, November 1975.
16. Avara, Elton P., "On the Spectrum Analysis of Binary Data," ECOM-5580, November 1975.
17. Taylor, Fredrick J., Thomas H. Pries, and Chao-Huan Huang, "Optimal Wind Velocity Estimation," ECOM-5581, December 1975.
18. Avara, Elton P., "Some Effects of Autocorrelated and Cross-Correlated Noise on the Analysis of Variance," ECOM-5582, December 1975.
19. Gillespie, Patti S., R.L. Armstrong, and Kenneth O. White, "The Spectral Characteristics and Atmospheric CO_2 Absorption of the Ho^{+3}:YLF Laser at 2.05μm," ECOM-5583, December 1975.
20. Novlan, David J., "An Empirical Method of Forecasting Thunderstorms for the White Sands Missile Range," ECOM-5584, February 1976.
21. Avara, Elton P., "Randomization Effects in Hypothesis Testing with Autocorrelated Noise," ECOM-5585, February 1976.
22. Watkins, Wendell R., "Improvements in Long Path Absorption Cell Measurement," ECOM-5586, March 1976.

23. Thomas, Joe, George D. Alexander, and Marvin Dubbin, "SATTEL — An Army Dedicated Meteorological Telemetry System," ECOM-5587, March 1976.
24. Kennedy, Bruce W. and Delbert Bynum, "Army User Test Program for the RDT&E-XM-75 Meteorological Rocket," ECOM-5588, April 1976.
25. Barnett, Kenneth M., "A Description of the Artillery Meteorological Comparisons at White Sands Missile Range, October 1974 — December 1974 ('PASS' — Prototype Artillery [Meteorological] Subsystem)," ECOM-5589, April 1976.
26. Miller, Walter B., "Preliminary Analysis of Fall-of-Shot From Project 'PASS'," ECOM-5590, April 1976.
27. Avara, Elton P., "Error Analysis of Minimum Information and Smith's Direct Methods for Inverting the Radiative Transfer Equation," ECOM-5591, April 1976.
28. Yee, Young P., James D. Horn, and George Alexander, "Synoptic Thermal Wind Calculations from Radiosonde Observations Over the Southwestern United States," ECOM-5592, May 1976.
29. Duncan, Louis D. and Mary Ann Seagraves, "Applications of Empirical Corrections to NOAA-4 VTPR Observations," ECOM-5593, May 1976.
30. Miers, Bruce T. and Steve Weaver, "Applications of Meterological Satellite Data to Weather Sensitive Army Operations," ECOM-5594, May 1976.
31. Sharenow, Moses, "Redesign and Improvement of Balloon ML-566," ECOM-5595, June 1976.
32. Hansen, Frank V., "The Depth of the Surface Boundary Layer," ECOM-5596, June 1976.
33. Pinnick, R.G. and E.B. Stenmark, "Response Calculations for a Commercial Light-Scattering Aerosol Counter," ECOM-5597, July 1976.
34. Mason, J. and G.B. Hoidale, "Visibility as an Estimator of Infrared Transmittance," ECOM-5598, July 1976.
35. Bruce, Rufus E., Louis D. Duncan, and Joseph H. Pierluissi, "Experimental Study of the Relationship Between Radiosonde Temperatures and Radiometric-Area Temperatures," ECOM-5599, August 1976.
36. Duncan, Louis D., "Stratospheric Wind Shear Computed from Satellite Thermal Sounder Measurements," ECOM-5800, September 1976.
37. Taylor, F., P. Mohan, P. Joseph and T. Pries, "An All Digital Automated Wind Measurement System," ECOM-5801, September 1976.
38. Bruce, Charles, "Development of Spectrophones for CW and Pulsed Radiation Sources," ECOM-5802, September 1976.
39. Duncan, Louis D. and Mary Ann Seagraves, "Another Method for Estimating Clear Column Radiances," ECOM-5803, October 1976.
40. Blanco, Abel J. and Larry E. Traylor, "Artillery Meteorological Analysis of Project Pass," ECOM-5804, October 1976.
41. Miller, Walter and Bernard Engebos, "A Mathematical Structure for Refinement of Sound Ranging Estimates," ECOM-5805, November, 1976.
42. Gillespie, James B. and James D. Lindberg, "A Method to Obtain Diffuse Reflectance Measurements from 1.0 to 3.0μm Using a Cary 17I Spectrophotometer," ECOM-5806, November 1976.
43. Rubio, Roberto and Robert O. Olsen, "A Study of the Effects of Temperature Variations on Radio Wave Absorption," ECOM-5807, November 1976.
44. Ballard, Harold N., "Temperature Measurements in the Stratosphere from Balloon-Borne Instrument Platforms, 1968-1975," ECOM-5808, December, 1976.
45. Monahan, H.H., "An Approach to the Short-Range Prediction of Early Morning Radiation Fog," ECOM-5809, January 1977.
46. Engebos, Bernard Francis, "Introduction to Multiple State Multiple Action Decision Theory and Its Relation to Mixing Structures," ECOM-5810, January 1977.
47. Low, Richard D.H., "Effects of Cloud Particles on Remote Sensing from Space in the 10-Micrometer Infrared Region," ECOM-5811, January 1977.

DISTRIBUTION LIST

Commanding Officer
Picatinny Arsenal
ATTN: SARPA-TS-S, #59
Dover, NJ 07801

Commanding Officer
Harry Diamond Laboratory
ATTN: Library
2800 Powder Mill Road
Adelphi, MD 20783

Commander
US Army Electronics Command
ATTN: DRSEL-RD-D
Fort Monmouth, NJ 07703

Naval Surface Weapons Center
Code DT 21 (Ms. Greeley)
Dahlgren, VA 22448

Air Force Weapons Laboratory
ATTN: Technical Library (SUL)
Kirtland AFB, NM 87117

Director
US Army Engr Waterways Exper Sta
ATTN: Library Branch
Vicksburg, MS 39180

Commander
US Army Electronics Command
ATTN: DRSEL-CT-D
Fort Monmouth, NJ 07703

Meteorologist in Charge
Kwajalein Missile Range
PO Box 67
APO
San Francisco, CA 96555

Environmental Protection Agency
Meteorology Laboratory
Research Triangle Park, NC 27711

Chief, Technical Services Div
DCS/Aerospace Sciences
ATTN: AWS/DNTI
Scott AFB, IL 62225

Air Force Cambridge Rsch Labs
ATTN: LCH (A. S. Carten, Jr.)
Hanscom AFB
Bedford, MA 01731

Department of the Air Force
16WS/DO
Fort Monroe, VA 23651

Director
US Army Ballistic Research Lab
ATTN: DRXBR-AM
Aberdeen Proving Ground, MD 21005

Geophysics Division
Code 3250
Pacific Missile Test Center
Point Mugu, CA 93042

National Center for Atmos Res
NCAR Library
PO Box 3000
Boulder, CO 80303

William Peterson
Research Association
Utah State University, UNC 48
Logan, UT 84322

Commander
US Army Dugway Proving Ground
ATTN: MT-S
Dugway, UT 84022

Head, Rsch and Development Div (ESA-131)
Meteorological Department
Naval Weapons Engineering Support Act
Washington, DC 20374

Commander
US Army Electronics Command
ATTN: DRCDE-R
5001 Eisenhower Avenue
Alexandria, VA 22304

Marine Corps Dev & Educ Cmd
Development Center
ATTN: Cmd, Control, & Comm Div (C^3)
Quantico, VA 22134

Commander
US Army Electronics Command
ATTN: DRSEL-WL-D1
Fort Monmouth, NJ 07703

Commander
US Army Missile Command
ATTN: DRSMI-RFGA, B. W. Fowler
Redstone Arsenal, AL 35809

Dir of Dev & Engr
Defense Systems Div
ATTN: SAREA-DE-DDR
H. Tannenbaum
Edgewood Arsenal, APG, MD 21010

Mr. William A. Main
USDA Forest Service
1407 S. Harrison Road
East Lansing, MI 48823

Naval Surface Weapons Center
Technical Library and Information
Services Division
White Oak, Silver Spring, MD 20910

Dr. A. D. Belmont
Research Division
PO Box 1249
Control Data Corp
Minneapolis, MN 55440

Dir, Elec Tech and Devices Lab
US Army Electronics Command
ATTN: DRSEL-TL-D, Bldg 2700
Fort Monmouth, NJ 07703

Director
Development Center MCDEC
ATTN: Firepower Division
Quantico, VA 22134

Commander
US Army Proving Ground
ATTN: Technical Library, Bldg 2100
Yuma, AZ 85364

US Army Liaison Office
MIT-Lincoln Lab, Library A-082
PO Box 73
Lexington, MA 02173

Library-R-51-Tech Reports
Environmental Research Labs
NOAA
Boulder, CO 80302

Head, Atmospheric Research Section
National Science Foundation
1800 G. Street, NW
Washington, DC 20550

Commander
US Army Missile Command
ATTN: DRSMI-RR
Redstone Arsenal, AL 35809

Commandant
US Army Field Artillery School
ATTN: Met Division
Fort Sill, OK 73503

Meteorology Laboratory
AFCRL/LY
Hanscom AFB
Bedford, MA 01731

Commander
US Army Engineer Topographic Lab
(STINFO CENTER)
Fort Belvoir, VA 22060

Commander
US Army Missile Command
ATTN: DRSMI-RRA, Bldg 7770
Redstone Arsenal, AL 35809

Air Force Avionics Lab
ATTN: AFAL/TSR
Wright-Patterson AFB, Ohio 45433

Commander
US Army Electronics Command
ATTN: DRSEL-VL-D
Fort Monmouth, NJ 07703

Commander
USAICS
ATTN: ATSI-CTD-MS
Fort Huachuca, AZ 85613

E&R Center
Bureau of Reclamation
ATTN: Bldg 67, Code 1210
Denver, CO 80225

HQDA (DAEN-RDM/Dr. De Percin)
Forrestal Bldg
Washington, DC 20314

Commander
Air Force Weapons Laboratory
ATTN: AFWL/WE
Kirtland AFB, NM 87117

Commander
US Army Satellite Comm Agc
ATTN: DRCPM-SC-3
Fort Monmouth, NJ 07703

Commander
US Army Electronics Command
ATTN: DRSEL-MS-TI
Fort Monmouth, NJ 07703

Commander
US Army Electronics Command
ATTN: DRSEL-GG-TD
Fort Monmouth, NJ 07703

Dr. Robert Durrenberger
Dir, The Lab of Climatology
Arizona State University
Tempe, AZ 85281

Commander
Headquarters, Fort Huachuca
ATTN: Tech Ref Div
Fort Huachuca, AZ 85613

Field Artillery Consultants
1112 Becontree Drive
ATTN: COL Buntyn
Lawton, OK 73501

Commander
US Army Nuclear Agency
ATTN: ATCA-NAW
Building 12
Fort Bliss, TX 79916

Director
Atmospheric Physics & Chem Lab
Code 31, NOAA
Department of Commerce
Boulder, CO 80302

Dr. John L. Walsh
Code 5503
Navy Research Lab
Washington, DC 20375

Commander
US Army Air Defense School
ATTN: C&S Dept, MSLSCI Div
Fort Bliss, TX 79916

Director National Security Agency
ATTN: TDL (C513)
Fort George G. Meade, MD 20755

USAF EPAC/CBT (Stop 825)
ATTN: Mr. Burgmann
Scott AFB, IL 62225

Armament Dev & Test Center
ADTC (DLOSL)
Eglin AFB, Florida 32542

Commander
US Army Ballistic Rsch Labs
ATTN: DRXBR-IB
Aberdeen Proving Ground, MD 21005

Director
Naval Research Laboratory
Code 2627
Washington, DC 20375

Commander
Naval Elect Sys Cmd HQ
Code 51014
Washington, DC 20360

The Library of Congress
ATTN: Exchange & Gift Div
Washington, DC 20540
2

CO, US Army Tropic Test Center
ATTN: STETC-MO-A (Tech Lib)
APO New York 09827

Commander
Naval Electronics Lab Center
ATTN: Library
San Diego, CA 92152

Office, Asst Sec Army (R&D)
ATTN: Dep for Science & Tech
Hq, Department of the Army
Washington, DC 20310

Director
US Army Ballistic Research Lab
ATTN: DRXBR-AM, Dr. F. E. Niles
Aberdeen Proving Ground, MD 21005

Commander
Frankford Arsenal
ATTN: Library, K2400, Bldg 51-2
Philadelphia, PA 19137

Director
US Army Ballistic Research Lab
ATTN: DRXBR-XA-LB
Bldg 305
Aberdeen Proving Ground, MD 21005

Dir, US Naval Research Lab
Code 5530
Washington, DC 20375

Commander
Office of Naval Research
Code 460-M
Arlington, VA 22217

Commander
Naval Weather Service Command
Washington Navy Yard
Bldg 200, Code 304
Washington, DC 20374

Technical Processes Br
D823
Room 806, Libraries Div NOAA
8060 13th St
Silver Spring, MD 20910

The Environmental Rsch Institute of MI
ATTN: IRIA Library
PO Box 618
Ann Arbor, MI 48107

Redstone Scientific Info Center
ATTN: Chief, Documents
US Army Missile Command
Redstone Arsenal, AL 35809

Commander
Edgewood Arsenal
ATTN: SAREA-TS-L
Aberdeen Proving Ground, MD 21010

Sylvania Elec Sys Western Div
ATTN: Technical Reports Library
PO Box 205
Mountain View, CA 94040

Commander
US Army Security Agency
ATTN: IARD-OS
Arlington Hall Station
Arlington, VA 22212
2

President
US Army Field Artillery Board
Fort Sill, OK 73503

Commandant
US Army Field Artillery School
ATTN: ATSF-TA-R
Fort Sill, OK 73503

CO, USA Foreign Sci & Tech Center
ATTN: DRXST-ISI
220 7th Street, NE
Charlottesville, VA 22901

Commander, Naval Ship Sys Cmd
Technical Library, Rm 3 S-08
National Center No. 3
Washington, DC 20360

Commandant
US Army Signal School
ATTN: ATSN-CD-MS
Fort Gordon, GA 30905

Rome Air Development Center
ATTN: Documents Library
TILD (Bette Smith)
Griffiss Air Force Base, NY 13441

HQ, ESD/DRI/S-22
Hanscom AFB
MA 01731

Commander
Frankford Arsenal
ATTN: J. Helfrich PDSP 65-1
Philadelphia, PA 19137

Director
Defense Nuclear Agency
ATTN: Tech Library
Washington, DC 20305

Department of the Air Force
5WW/DOX
Langley AFB, VA 23665

Commander
US Army Missile Command
ATTN: DRSMI-RER (Mr. Haraway)
Redstone Arsenal, AL 35809

CPT Hugh Albers, Exec Sec
Interdept Committee on Atmos Sci
Fed Council for Sci & Tech
National Sci Foundation
Washington, DC 20550

US Army Research Office
ATTN: DRXRO-IP
PO Box 12211
Research Triangle Park, NC 27709

Commander
US Army Training & Doctrine Cmd
ATTN: ATCD-SC
Fort Monroe, VA 23651

Mil Assistant for Environmental Sciences
OAD (E & LS), 3D129
The Pentagon
Washington, DC 20301

Commander
Eustis Directorate
US Army Air Mobility R&D Lab
ATTN: Technical Library
Fort Eustis, VA 23604

National Weather Service
National Meteorological Center
World Weather Bldg - 5200 Auth Rd
ATTN: Mr. Quiroz
Washington, DC 20233

Commander
US Army Materiel Command
ATTN: DRCRD-SS (Mr. Andrew)
Alexandria, VA 22304

Commander
Frankford Arsenal
ATTN: SARFA-FCD-O, Bldg 201-2
Bridge & Tarcony Sts
Philadelphia, PA 19137

Inge Dirmhirn, Professor
Utah State University, UMC 48
Logan, UT 84322

Chief, Aerospace Environ Div
Code ES41
NASA
Marshall Space Flight Center, AL 35802

Dr. Frank D. Eaton
PO Box 3038
University Station
Laramie, Wyoming 82071

Commander
US Army Arctic Test Center
ATTN: STEAC-OP-PL
APO Seattle 98733

Commander
US Army Electronics Command
ATTN: DRSEL-GS-H (Stevenson)
Fort Monmouth, NJ 07703

Commander
USACACDA
ATTN: ATCA-CCC-W
Fort Leavenworth, KS 66027

Commander
US Army Test & Eval Cmd
ATTN: DRSTE-FA
Aberdeen Proving Ground, MD 21005

Air Force Cambridge Rsch Labs
ATTN: LKI
L. G. Hanscom Field
Bedford, MA 01730

Director, Systems R&D Service
Federal Aviation Administration
ATTN: ARD-54
2100 Second Street, SW
Washington, DC 20590

USAFETAC/CB (Stop 825)
Scott AFB
IL 62225

Director
USAE Waterways Experiment Station
ATTN: Library
PO Box 631
Vicksburg, MS 39180

Defense Documentation Center
ATTN: DDC-TCA
Cameron Station (BLDG 5)
Alexandria, Virginia 22314
12

Commander
US Army Electronics Command
ATTN: DRSEL-CT-S
Fort Monmouth, NJ 07703

Commander
Holloman Air Force Base
6585 TG/WE
Holloman AFB, NM 88330

Commandant
USAFAS
ATTN: ATSF-CD-MT (Mr. Farmer)
Fort Sill, OK 73503
2

Commandant
USAFAS
ATTN: ATSF-CD-C (Mr. Shelton)
Fort Sill, OK 73503
2

Commander
US Army Electronics Command
ATTN: DRSEL-CT-S (Dr. Swingle)
Fort Monmouth, NJ 07703
3

☆ U.S. GOVERNMENT PRINTING OFFICE: 1977—777-022/9